Atmospheric Environment 167 (2017) 586–602

Contents lists available at ScienceDirect

Atmospheric Environment

journal homepage: www.elsevier.com/locate/atmosenv

The pulsating nature of large-scale Saharan dust transport as a result of interplays between mid-latitude Rossby waves and the North African Dipole Intensity

E. Cuevas [a, *], A.J. Gómez-Peláez [a], S. Rodríguez [a], E. Terradellas [b], S. Basart [c], R.D. García [a, d], O.E. García [a], S. Alonso-Pérez [e]

[a] Izaña Atmospheric Research Centre (AEMET), c/ La Marina 20, 38001 Santa Cruz de Tenerife, Spain
[b] SDS-WAS Regional Centre (AEMET), Edificio Nexus II, c/ Jordi Girona 29, 08034 Barcelona, Spain
[c] Earth Sciences Department, Barcelona Supercomputing Centre, Edificio Nexus II, c/ Jordi Girona 29, 08034 Barcelona, Spain
[d] Air Liquide S.A., Delegación de Canarias, Plaza Industrial Valle Güímar Manz, 38500 Güímar, Santa Cruz de Tenerife, Spain
[e] Universidad Europea de Canarias, Campus de la Orotava, c/ Inocencio García 1, 38300 La Orotava, Santa Cruz de Tenerife, Spain

HIGHLIGHTS

- Saharan dust transport out of Africa shows a pulsed behaviour.
- The North African Dipole Intensity (NAFDI) modulates Saharan dust export.
- NAFDI intra-seasonal variations are driven by mid-latitude Rossby waves.
- NAFDI drives the temporal evolution of the Saharan Heat Low longitudinal shift.
- NAFDI may modulate dust emission in central-western Sahara.

ARTICLE INFO

Article history:
Received 13 April 2017
Received in revised form
25 August 2017
Accepted 28 August 2017
Available online 30 August 2017

Keywords:
NAFDI
Rossby waves
SHL
Sahara
Dust
MODIS AOD
Atmospheric dynamics

ABSTRACT

It was previously shown that during August the export of Saharan dust to the Atlantic was strongly affected by the difference of the 700-hPa geopotential height anomaly between the subtropics and the tropics over North Africa, which was termed the North African Dipole Intensity (NAFDI). In this work a more comprehensive analysis of the NAFDI is performed, focusing on the entire summer dust season (June–September), and examining the interactions between the mid-latitude Rossby waves (MLRWs) and NAFDI. Widespread and notable aerosol optical depth (AOD) monthly anomalies are found for each NAFDI-phase over the dust corridors off the Sahara, indicating that NAFDI presents intra-seasonal variability and drives dust transport over both the Mediterranean basin and the North Atlantic. Those summer months with the same NAFDI-phase show similar AOD-anomaly patterns. Variations in NAFDI-phase also control the displacement of the Saharan Heat Low (SHL) westwards or eastwards through horizontal advection of temperature over Morocco-Western Sahara or eastern Algeria-Western Libya, respectively. The connection between the SHL and the NAFDI is quantified statistically by introducing two new daily indexes that account for their respective phases (NAFDI daily index -NAFDIDI-, and SHL longitudinal shift index -SHLLSI-) and explained physically using the energy equation of the atmospheric dynamics. The Pearson's correlation coefficient between the one–day-lag SHLLSI and the NAFDIDI for an extended summer season (1980–2013) is 0.78. A positive NAFDI is associated with the West-phase of the SHL, dust sources intensification on central Algeria, and positive AOD anomalies over this region and the Subtropical North Atlantic. A negative NAFDI is associated with the East-phase of the SHL, and positive AOD anomalies over central-eastern Sahara and the central-western Mediterranean Sea. The results point out that the phase changes of NAFDI at intra-seasonal time scale are conducted by those MLRWs that penetrate deeply into the low troposphere.

* Corresponding author.
E-mail address: ecuevasa@aemet.es (E. Cuevas).

http://dx.doi.org/10.1016/j.atmosenv.2017.08.059

1. Introduction

Mineral dust from deserts is the second most important contributor to the global atmospheric aerosol burden after sea-salt aerosols (Huneeus et al., 2013 and references herein). The largest and most active dust source worldwide is the Sahara desert (i.e., Ginoux et al., 2012; Goudie and Middleton, 2001) with an emission range between 400 and 2200 Tg yr^{-1}. Dust impacts on climate (i.e. Foltz and McPhaden, 2008; Prospero and Lamb, 2003; Tegen and Torres, 2005), air quality (e.g., Prospero, 1999; Prospero et al., 2014) and health (e.g., Díaz et al., 2012; Karanasiou et al., 2012; Prospero and Lamb, 2003). The Saharan Air Layer (SAL), usually heavily laden with mineral dust, reaches regions as far away as the Caribbean and the Americas (e.g., Adams et al., 2012; Gläser et al., 2015; Perry et al., 1997; Prospero and Carlson, 1972). Dust also reaches the Mediterranean basin (Basart et al., 2009; Moulin et al., 1998) with implication even in the compliance of European air quality standards (Escudero et al., 2007; Marconi et al., 2014; Rodríguez et al., 2001). In the Sahel region, dust is associated with meningitis epidemics during the dry season (Pérez García-Pando et al., 2014; Thomson et al., 2006). Concerning ecosystems, the Saharan dust deposition fertilises the Amazon rainforest (Yu et al., 2015) and triggers marine phytoplankton growth in both the North Atlantic (Ravelo-Pérez et al., 2016) and the Mediterranean Sea (Gallisai et al., 2014), playing a key subsequent role in controlling the chemical composition of sea-water and hence in the carbon cycle (Conway and John, 2014).

Given this wide variety of impacts, a good knowledge of Saharan dust outflows variability at different spatiotemporal scales is absolutely essential to assess the variability induced by Saharan dust in changes observed in climate, air quality, and ecosystems, as well as to improve operational forecasting capabilities to predict dust storms (Benedetti et al., 2014; Huneeus et al., 2011; Stein et al., 2015).

African dust emission and transport exhibits a high variability from diurnal (Cuesta et al., 2009) to multi-decadal time scales (Wang et al., 2015; Evan et al., 2016). The seasonal variation of Saharan dust outflows has been reasonably well studied in affected regions (Barnaba and Gobbi, 2004; Israelevich et al., 2012; Prospero et al., 2014, and references therein). Tegen (2013) investigated the role of the atmospheric circulation in the inter-annual variability of dust source activation frequency. Inter-annual dust outflows variations are relatively well known in the winter period (Nakamae and Shiotani, 2013), which are mostly associated with the North Atlantic Oscillation (Chiapello et al., 2005; Ginoux et al., 2004). However, only in recent years research on inter-annual variations of Saharan dust outflows during the summer period has been carried out (i.e., Ben-Ami et al., 2009; Engelstaedter et al., 2009; Rodríguez et al., 2015). In this season Saharan dust mobilization shows its peak (Engelstaedter and Washington, 2007).

Rodríguez et al. (2015) introduced the North African Dipole Intensity (NAFDI) index, which is the difference of the 700-hPa geopotential height (Z700) anomalies averaged over the subtropical (30-32°N, Morocco) and the tropical (10-13°N, Bamako) North Africa regions close to the Atlantic coast (at 5-8°W). These authors used satellite Aerosol Index and the 28-year-long in-situ dust concentration record at the high-mountain Izaña Observatory to explain the influence of changes in the NAFDI intensity to the dust outflows from west Sahara to the tropical Atlantic in August. Note that a similar approach was applied later to account for dust transport in southwest Asia with the Caspian Sea-Hindu Kush Index (CasHKI) (Kaskaoutis et al., 2016). Since inter-annual variability in dust outflows towards the North Atlantic is observed (Rodríguez et al., 2015), it seems reasonable to expect a certain relationship between NAFDI and dust emissions over the Sahara. On the other hand, Rodríguez et al. (2015) did not determine whether the NAFDI and associated dust outflows show intra-seasonal variations whereas it is well known that dust transport occurs in the form of strong pulses along the Mediterranean-Europe-Middle-East and North-Atlantic-Caribbean-North-America routes (Guerzoni et al., 1999; Prospero, 1996; Prospero and Mayol-Bracero, 2003). In this paper we answer the following question: what atmospheric processes produce the pulsed behaviour of dust outflows observed at the intra-seasonal time scale?

It is well known that changes in the strength and location of the Saharan heat low (SHL) (Lavaysse et al., 2009) constitute a crucial issue for understanding regional dust mobilization because changes in the SHL are tightly linked to the activation of some key meso-scale processes such as density currents, low-level jets (LLJ), and severe convective phenomena present in the equatorial convergence zone (Allen and Washington, 2013; Knippertz and Todd, 2010; Lavaysse et al., 2010a; Marsham et al., 2013; Roehrig et al., 2011). Since the SHL is associated with dust mobilization processes over the Sahara and NAFDI drives Saharan dust transport out of Africa, the following questions arise: 1) Is there a statistically significant relationship between the SHL-phase changes and the intra-seasonal variations we might find in NAFDI?; 2) If so, which of them acts as a driver of the other, and through which physical mechanism? On the other hand, the SHL is also a central meteorological system associated to the West African monsoon (Sultan and Janicot, 2003), which interacts with mid-latitude circulation (Chauvin et al., 2010; Knippertz, 2008, 2010; Lavaysse et al., 2010b; Roehrig et al., 2011). However, the specific reasons that might explain the SHL shifts and changes in intensity as well as in the associated atmospheric dust loadings are still poorly understood (Engelstaedter et al., 2015). According to Chauvin et al. (2010), the longitudinal position of the SHL is linked to the propagation of mid-latitude Rossby waves (MLRWs) over North Africa. However, these authors did not explore in detail nor identify the subjacent atmospheric processes behind that statistical relation. Therefore, we wonder about the role that MLRWs might play in the intra-seasonal variability of NAFDI, and if it is possible to explain the mechanisms that control the interaction between Rossby waves and the NAFDI and SHL phases.

To properly address these questions we set the following objectives in this study: 1) investigate intra-seasonal changes in dust transport over the Sahara and outflow regions driven by changes in NAFDI during summertime (June–September; hereinafter denoted as JJAS); 2) identify and analyse the atmospheric processes which might connect NAFDI variations with changes in the SHL position; and 3) identify and quantify the atmospheric physical mechanisms by which MLRWs might modulate at intra-seasonal scale the SHL-phase, and presumably also the NAFDI variations.

The satellite-based observations and reanalysis fields used in this study are detailed in section 2. In section 3, the main results are presented and discussed: relationships between NAFDI phases and specific patterns of dust transport and meteorological fields, as well as physical interactions between the NAFDI, the SHL and MLRWs. Finally, the conclusions are summarized in Section 4.

2. Data and methodology

2.1. MACC reanalysis

The 2003–2012 MACC (Monitoring Atmospheric Composition & Climate) reanalysis has been used in the present study. This reanalysis, described in Inness et al. (2013), can be downloaded from the http://apps.ecmwf.int/datasets/data/macc-reanalysis/levtype=sfc/ site from the ECMWF (European Centre for Medium-Range Weather Forecasts). AOD at 550 nm and derived estimated

instantaneous dust emission at 06, 09, 12, 15 and 18 UTC for JJAS in the period 2003–2012 have been used in our analysis. Dust emission is not provided by MACC reanalysis and has been estimated following the method described in Section 3.2.3.

A description of the reanalysis aerosol modules is provided by Benedetti et al. (2009), and Morcrette et al. (2009, 2011). The MACC reanalysis has been extensively used and validated in several studies on aerosols (Bellouin et al., 2013; Cesnulyte et al., 2014; Eskes et al., 2015; Inness et al., 2013) and mineral dust (Cuevas et al., 2015) studies.

2.2. MODIS data

The MODIS (MODerate resolution Imaging Spectrometer) provides aerosol data over both land and ocean (Kaufman et al., 1997; Tanré et al., 1997) at global scale on a daily basis.

For this study AOD (at 500 nm) monthly means from the MODIS-Collection 6 in the period 2003–2012 for JJAS have been used. MODIS-Collection 6 provides a new product, obtained by merging Deep Blue (DB) and Dark Target (DT) datasets. This new product allows to extend the coverage to bright lands as well as vegetated surfaces (Sayer et al., 2013). MODIS-Collection 6 dataset is particularly important in our analysis since large areas of the considered geographic domain (Northern Africa) show high reflectivity, where the AOD retrieval is not an easy task. MODIS-Collection 6 is available at ftp://ladsweb.nascom.nasa.gov/allData/6/.

2.3. NCEP/NCAR reanalysis

The NCEP (National Centre for Environmental Prediction) and the NCAR (National Centre for Atmospheric Research) cooperates producing reanalysed atmospheric fields for the research and climate monitoring communities (Kalnay et al., 1996).

NCEP/NCAR 6-hourly, daily, and monthly-mean data with a 2.5° lat. x 2.5° lon. resolution for JJAS, in the period 1980–2013, have been used in this study. In detail: monthly average fields of geopotential height at 700 hPa (m), wind vector and speed at 925 and 700 hPa (ms-1), and temperature at 925 hPa (K), within the 10°N-50°N, 50°W-40°E region, for the period 2003–2012 have been obtained. Monthly Omega fields at 300, 400, 500 and 600 hPa (Pas-1), and the zonal wind component at 300 hPa (ms-1) for the period 1980–2013, have been downloaded for the 5°N-70°N, 30°W-40°E domain. Monthly meridional and zonal wind components (ms-1) latitude/longitude-height cross-sections for specific longitudes/latitudes have been obtained. Monthly correlation plots between NAFDI and 200, 500, 700, 850 and 1000 hPa geopotential height fields, for the 0°N-90°N, 80°W-80°E domain, have been calculated for the period 1980–2013.

Daily NCEP/NCAR geopotential height at 700 hPa, temperature at 925, 850 and 700 hPa, Omega at 500 hPa, and zonal wind at 300 hPa, for the period 1980–2013, have been used to calculate the NAFDIDI (section 3.2.1), SHLLSI (section 3.2.1), OM500 (section 3.3) and WA300 (section 3.3) daily indexes, respectively.

NCEP NCAR reanalysis with the highest time resolution available (6-hourly, with data at 00, 06, 12 and 18 UTC), for the period 1980–2013, has been used to compute the terms of the energy-equation as explained in Supplement S7.

3. Results and discussion

3.1. Role of NAFDI in dust outflows and associated meteorological patterns

In this study we use the NAFDI concept established by Rodríguez et al. (2015). The two points chosen by those authors in the definition of the NAFDI were located over Mali and Morocco following the 7°W meridian because they wanted to analyse and characterize the transport of Saharan dust toward the North Atlantic. Since the Z700 s at these two points show a positive correlation (0.2–0.3, significant at the 80% level), the Z700 variations are not entirely independent from each other.

However, selecting the south point in the same parallel but shifted to the east (~5°E; Northern Nigeria), the flow anomaly is perpendicular to the line along which the NAFDI is computed (not shown), and therefore it can be accounted by the geostrophic wind anomaly associated to the geopotential height anomaly that defines NAFDI, and we obtain a zero correlation between the two Z700s. Therefore, in this paper, we use a new NAFDI monthly index (also called NAFDI) defined as the monthly Z700 anomaly between Morocco and Nigeria. An independent result that supports the proposed improvement is that the total in situ dust concentrations recorded at Izaña in August and the original long-term NAFDI data series in the period 1987–2014 (Rodríguez et al., 2015) present a Pearson's monthly correlation of 0.67 (significant at the 99.98% level), whereas it is equal to 0.72 (significant at the 99.997% level) with the improved NAFDI monthly index.

The new NAFDI index is used for categorizing months and subsequently average in time the associated MODIS AOD spatial fields and some dust transport-related atmospheric parameters. Specifically, we use NAFDI values for JJAS within the period 1980–2013. Taking into account the monthly-mean NAFDI value, we have classified the summer months into the following groups: negative (<−0.4), positive (>+0.4), and neutral (between −0.4 and + 0.4) NAFDI months. Considering the distribution of absolute monthly mean values, the neutral NAFDI region is delimited approximately by the 25th percentile. The spatial correlation plots shown in the Supplement of this paper are also computed using monthly means. Therefore, the critical value for having a significant Pearson's correlation with a 95% confidence level is 0.34.

The MODIS AOD mean anomaly field for each summer month and NAFDI-phase was calculated respect to the AOD mean field corresponding to all the occurrences of that summer month in the period 2003–2012. The AOD anomaly fields for JJAS for the positive and negative NAFDI phases are shown in Fig. 1. Extensive and notable AOD anomalies, associated outflows off the Sahara are notable. For positive NAFDI a broad positive ENE-WSW axis-shaped AOD anomaly over the subtropical North Atlantic (SNA) is observed, in agreement with results from Rodríguez et al. (2015), which showed a good relationship between TOMS/OMI Aerosol Index (AI) and NAFDI for August months. This positive AOD anomaly during positive NAFDI over the SNA is rather weak and small in June, sharpening notably in July and August, while in September a weakened contrast between positive and negative NAFDI is observed (Fig. 1).

For negative NAFDI, a second noteworthy pattern is observed in June over the tropical North Atlantic with a positive AOD anomaly, and strong negative AOD anomaly in the SNA in July and August, while September shows a neutral behaviour. A third major AOD-pattern contrast between the NAFDI phases is observed over the central-western Mediterranean (CWM) basin and southern Europe, where positive AOD anomalies are registered during negative NAFDI, and vice versa. This pattern is particularly unequivocal in June, when the highest frequencies of Saharan dust outbreaks into the CWM take place (Marconi et al., 2014).

It should be noted that within the same summer there are months showing both positive and negative NAFDI phases (intra-seasonal variation), which are also different from year to year (inter-annual variation). However, the AOD anomaly patterns are similar for all the summer months with the same NAFDI phases.

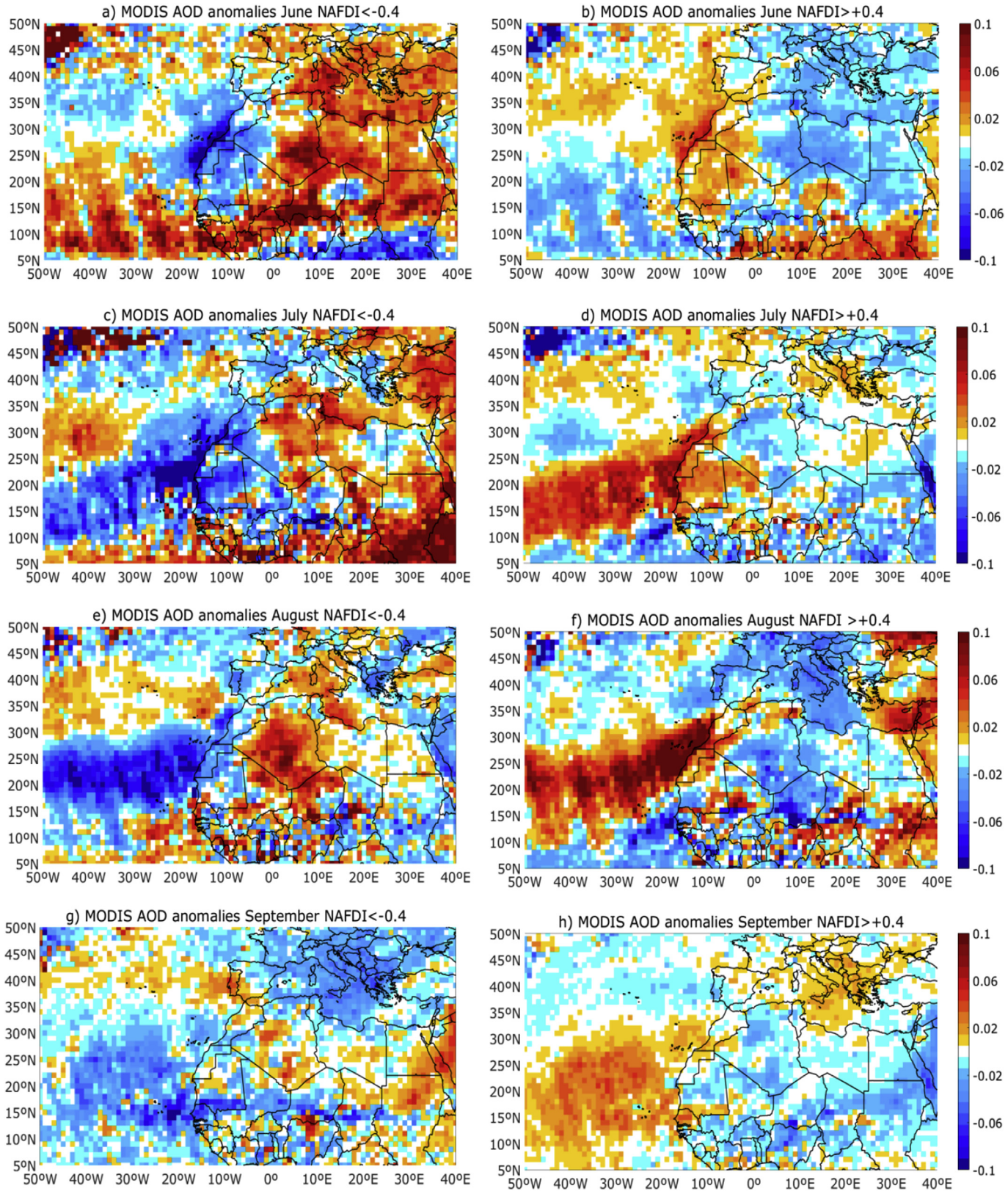

Fig. 1. AOD mean anomaly fields from MODIS (merged Deep-Blue and Dark-Target) for June, July, August, and September months with negative (a, c, e, and g) and positive (b, d, f, and h) NAFDI (2003–2012). (For interpretation of the references to colour in this figure legend, the reader is referred to the web version of this article.)

This suggests that the observed dust transport patterns may be driven by NAFDI, since the latter is associated with the large-scale wind anomaly in the lower troposphere over North-Western Africa. This relationship complements and extends previous results from Rodríguez et al. (2015). Moreover, we find positive AOD anomalies over central-western Sahara (CWS) dust sources, particularly over Algeria (Fig. 1) for positive NAFDI. The opposite is found for negative NAFDI. AOD anomalies from MACC reanalysis have been also obtained for each summer month in the same way as done for MODIS. The results, not taking into account small-scale details and the exact signal intensity, are quite similar to those obtained with MODIS for each NAFDI-phase (see Supplement S2). In the Sahel, the summer period is the rainy season in which frequent short-term convective meso-scale processes that raise huge amounts of dust take place (Marticorena et al., 2010). The high frequency of convective clouds in summertime in this region also implies a significantly lower daily AOD data availability, which may be the cause of the spatially highly variable means for both NAFDI phases over this region, in spite of the fact there is no significant (spatially consistent) correlation with NAFDI. If we take into account the fact that AOD positive anomalies over the SNA normally match up low AOD over the CWM, and vice versa, we can hypothesize that the same meteorological driver favours Saharan dust transport toward one region or another. Considering that Z700 is the most effective level for dust transport over the SNA (Rodríguez et al., 2015, and references therein), we explored the Z700 patterns corresponding to each NAFDI-phase. In June, July and August, and slightly less in September, we observe marked differences in the Z700 patterns corresponding to each phase (Fig. 2), with a significant strengthening of Z700 over Morocco for positive NAFDI. During negative NAFDI a deep SW-NE axis-shaped trough extends from the western edge of Europe and North Africa to the SNA.

This trough displaces further away the Azores high, which also become slightly elongated to the NE, from the North African high (at 700 hPa), being located the latter in a more Eastern position over the continent. Conversely, during the positive NAFDI-phase both anticyclones strengthen and get closer at 700 hPa, merging into an apparent single huge Azores high extending over much North Africa.

Gkikas et al. (2015) found a quite similar pattern, which accounts for, leastwise, 50% of all mineral dust intrusions in the entire Mediterranean basin (Cluster#2). The Z700 pattern found under negative NAFDI also agrees with that proposed by Varga et al. (2014) when discussing Saharan dust outbreaks into the CWM basin. The deeper trough present during negative NAFDI over the eastern North Atlantic at 700 hPa is also observed at other levels. Monthly correlation plots between the geopotential height fields, ranging from 200 to 1000 hPa, and NAFDI for summer months have been calculated (see Supplement S3). These plots show very similar correlation patterns at standard 850, 700, 500 and 200 hPa levels, and even vaguely at 1000 hPa. All these facts suggest that the NAFDI variations at intra-seasonal scale might be driven by MLRWs. The relationship between the NAFDI and MLRWs is addressed in Subsection 3.3.

The NCEP/NCAR monthly averaged wind plots at 700 hPa (Fig. 3) show relatively strong NE/ENE winds over the Western Sahara, northern Mauritania and central Algeria that extends into the SNA for positive NAFDI, mainly in July and August. This increase in north-easterly wind component over these regions for positive NAFDI is clearly seen in the wind anomalies at 700 hPa shown in Supplement S1. These results agree with the positive AOD anomaly detected by MODIS on these regions (Fig. 1).

Under negative NAFDI we observe an increase in airflow from North Africa to CWM and, simultaneously, stronger westerly winds over the Mediterranean region. The same consistency over time is observed for the period July–August 1980–2013 from monthly correlation fields between NAFDI and 700 hPa meridional (impact on the Mediterranean basin) and zonal (impact on the SNA) wind components (not shown here). Correlations between 700-hPa zonal wind and NAFDI of −0.7 are found over Western Sahara, Northern Mauritania, and central Algeria. Correlations between NAFDI and meridional wind of −0.7 are found over north-eastern Algeria, Tunisia and north-western Libya. These results indicate that the good correlations between NAFDI and the zonal wind toward the Atlantic Ocean and the meridional component toward the Mediterranean Sea constitute a permanent feature maintained over decades.

The associated 700-hPa wind field is weak over the CWS (Algeria and Western Sahara) in June and September (Fig. 3a, b, g and h) whereas in July and August it intensifies significantly with a clear easterly component during positive NAFDI (Fig. 3c, d, e and f). This is the reason for which the marked contrast between the AOD patterns for positive and negative NAFDI in July and August over the SNA is not observed in June and September.

The longitudinal variation of the zonal wind component in a vertical cross-section along 28°N, calculated from NCEP/NCAR reanalysis (Fig. 4), shows that in June the westerlies dominate (positive values) above the coast of Africa under both NAFDI phases, greatly hindering the transport of dusty air masses from the CWS convective boundary layer (CBL) (Cuesta et al., 2009) to the SNA. The same situation is found for the rest of the summer months under negative NAFDI. However, under positive NAFDI, in July and August, and to a lesser extent in September, the easterlies (negative zonal wind component) dominate from 700 to 900 hPa, favouring westwards intrusions of the SAL, and hence, transport of dusty air masses over the SNA. It should be noted that 28°N is the latitude of the Izaña Observatory where Rodríguez et al. (2015) observed in the free-troposphere maximum in-situ dust levels for positive NAFDI.

Concerning the Mediterranean basin, the latitudinal variation of the meridional wind component in a vertical cross-section along 9°E, calculated from NCEP/NCAR reanalysis (Fig. 5), shows that a predominant northerly wind component restrains the arrival of Saharan air masses into the CWM basin under positive NAFDI. Conversely, dust outbreaks into the CWM are favoured under negative NAFDI because of the existence of a dominant Southerly wind component above 900 hPa in June, which is also observed to a lesser extent in July and August, and very weakened in September. This result agrees with other studies that characterize the vertical structure of the SAL over the CWM (Marconi et al., 2014; Mona et al., 2006).

3.2. Statistical and physical connections between the NAFDI and the Saharan heat low longitudinal shift

We have found for each NAFDI phase specific spatial patterns of several key meteorological variables, which are quite similar to those found in Chauvin et al. (2010) for the SHL West and East phases, suggesting there could be a physical connection between the NAFDI and the location of the SHL. The most noteworthy are: 1) the location and spread of the Azores high; 2) the 925-hPa temperature anomaly over the Western Sahara and most of Morocco (Fig. 6); 3) the low-level winds over Libya, Morocco and Western Sahara.

There are some more indications about the relationship between NAFDI variations and longitudinal displacements of the SHL: when NAFDI is negative, the oceanic low-level (925 hPa) relatively-cold (compared with the surrounding area) southward flow reaching North Africa within the 10°W-20°W band (shown in Supplement S4) penetrates deeper in North Africa and comes from more northern latitudes. This flow produces a negative

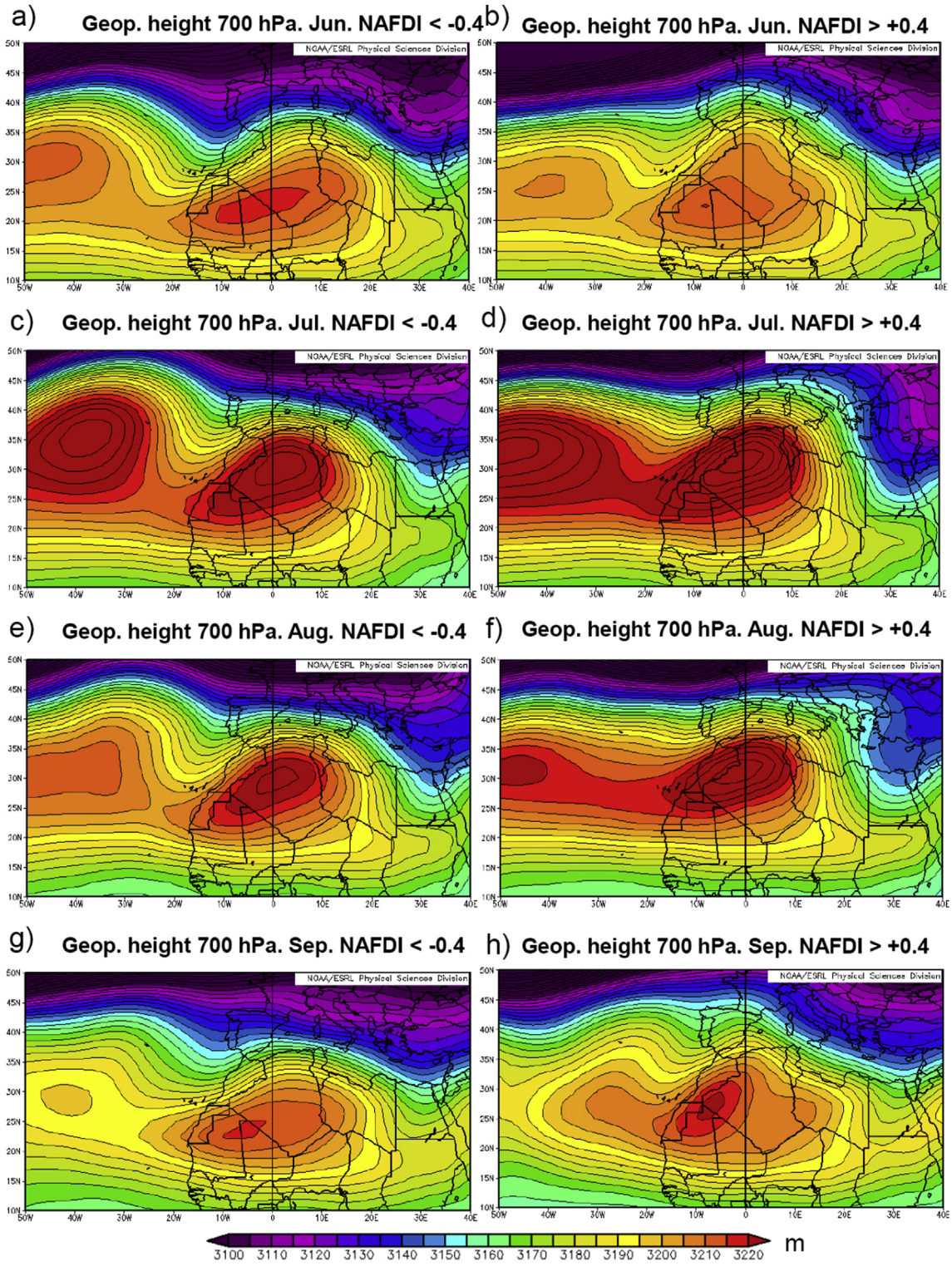

Fig. 2. Z700 (m) means for June, July, August, and September months with negative (a, c, e, and g) and positive (b, d, f, and h) NAFDI (2003–2012) from NCEP/NCAR reanalysis.

geopotential-thickness advection that causes a deep trough (Fig. 2), and cools the land surface over Morocco and Western Sahara (Fig. 6). This scenario likely contributes to maintain the SHL in its East phase. This is in agreement with finding a negative anomaly of the CBL height over Western Sahara and Morocco, and a positive CBL-height anomaly over eastern Algeria and north-western Libya for negative NAFDI (shown in Supplement S5).

The striking connection between the SHL and NAFDI phases is quantified and explained physically in this subsection.

3.2.1. Statistical relationship between NAFDI and SHL

Lavaysse et al. (2009) defined the WAHL (West African Heat Low) location using the Low-Level Atmospheric Thickness (LLAT), where low-level means the pressure range 925–700 hPa. The LLAT

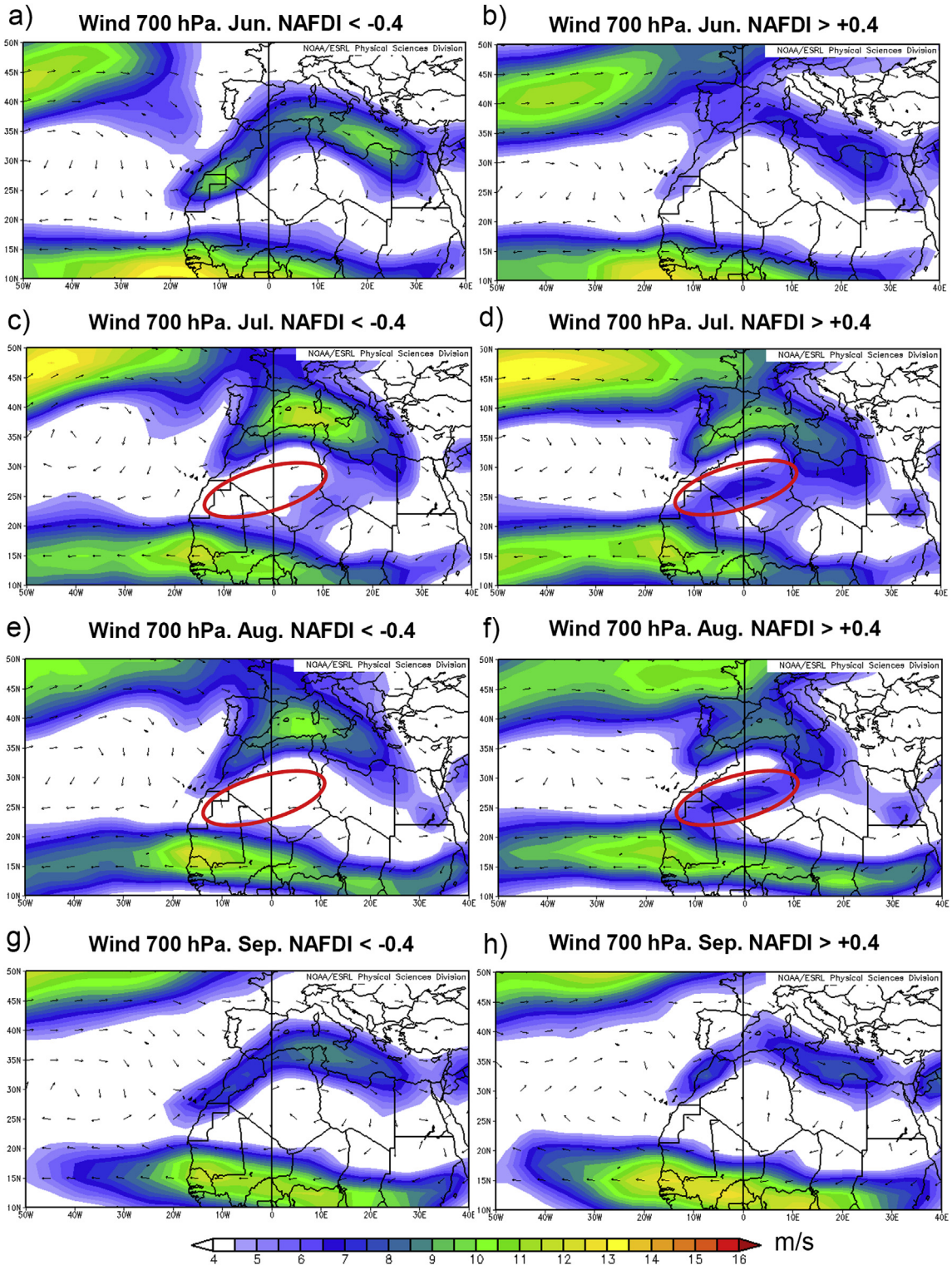

Fig. 3. 700-hPa wind (m s-1) means for June, July, August, and September months with negative (a, c, e and g) and positive (b, d, f and h) NAFDI (2003–2012) from NCEP/NCAR reanalysis. Encircled in red is the region comprising the Western Sahara, northern Mauritania and central Algeria where strengthened NE/ENE winds are observed in July and August for positive NAFDI. (For interpretation of the references to colour in this figure legend, the reader is referred to the web version of this article.)

depends linearly on the air average temperature between those pressure levels. Lavaysse et al. (2013) determined the longitudinal shift of the SHL (see their Fig. 5c and d) performing an Empirical Orthogonal Function analysis (EOF) carried out exclusively in the region where the SHL uses to be during the summer, being the time frequencies associated to the displacement higher than 1/25 day^{-1}.

Below it is shown that the evolution in time of the NAFDI and the longitudinal shift of the SHL are tightly linked on a daily basis. Positive NAFDI corresponds to the SHL West-phase, and negative NAFDI to the SHL East-phase.

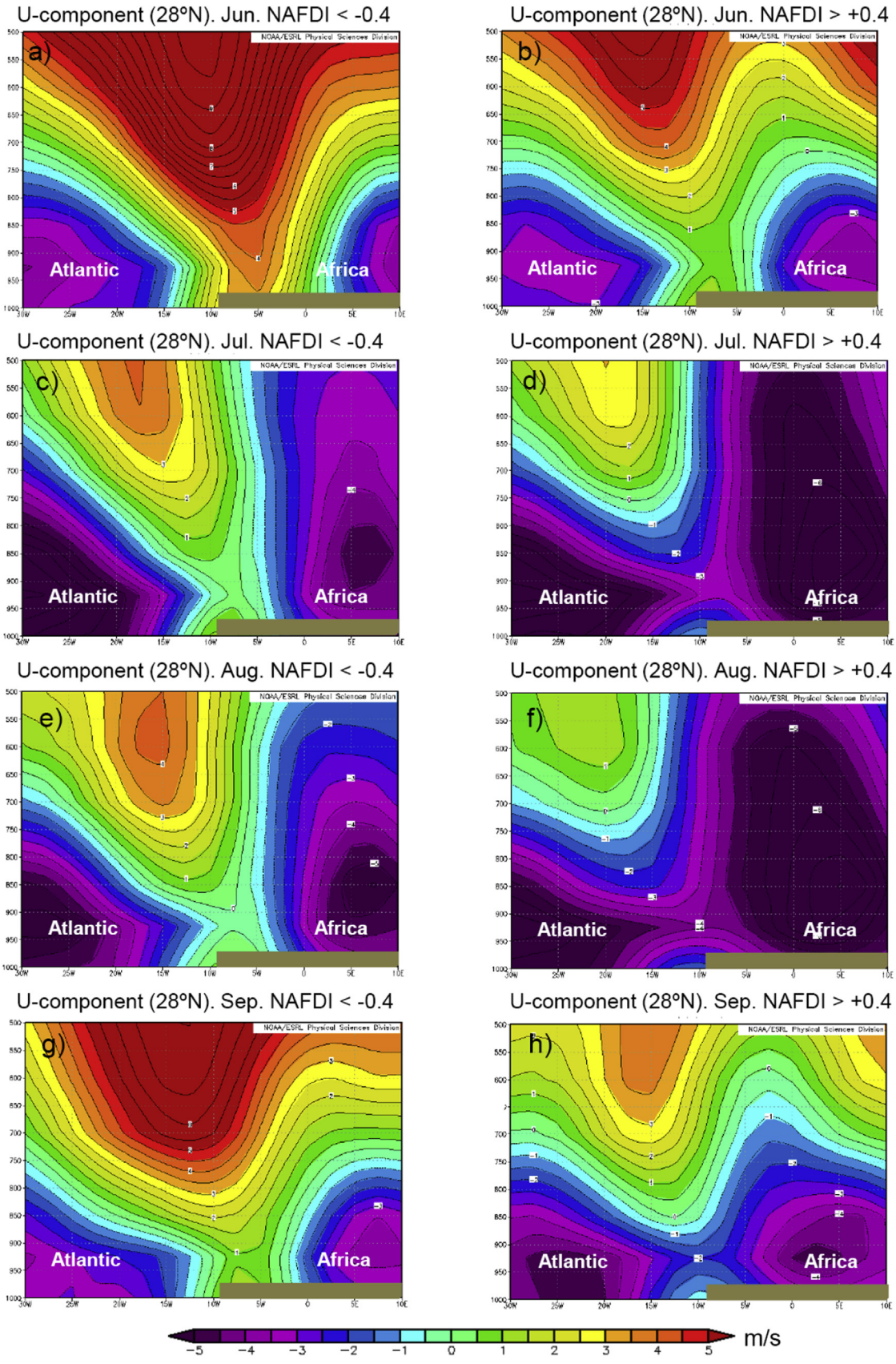

Fig. 4. Mean-zonal-wind-component (m s-1) longitude-height cross-sections along 28°N (CWS and SNA) for June, July, August, and September months with negative (a, c, e, and g) and positive (b, d, f, and h) NAFDI (2003–2012) from NCEP/NCAR reanalysis.

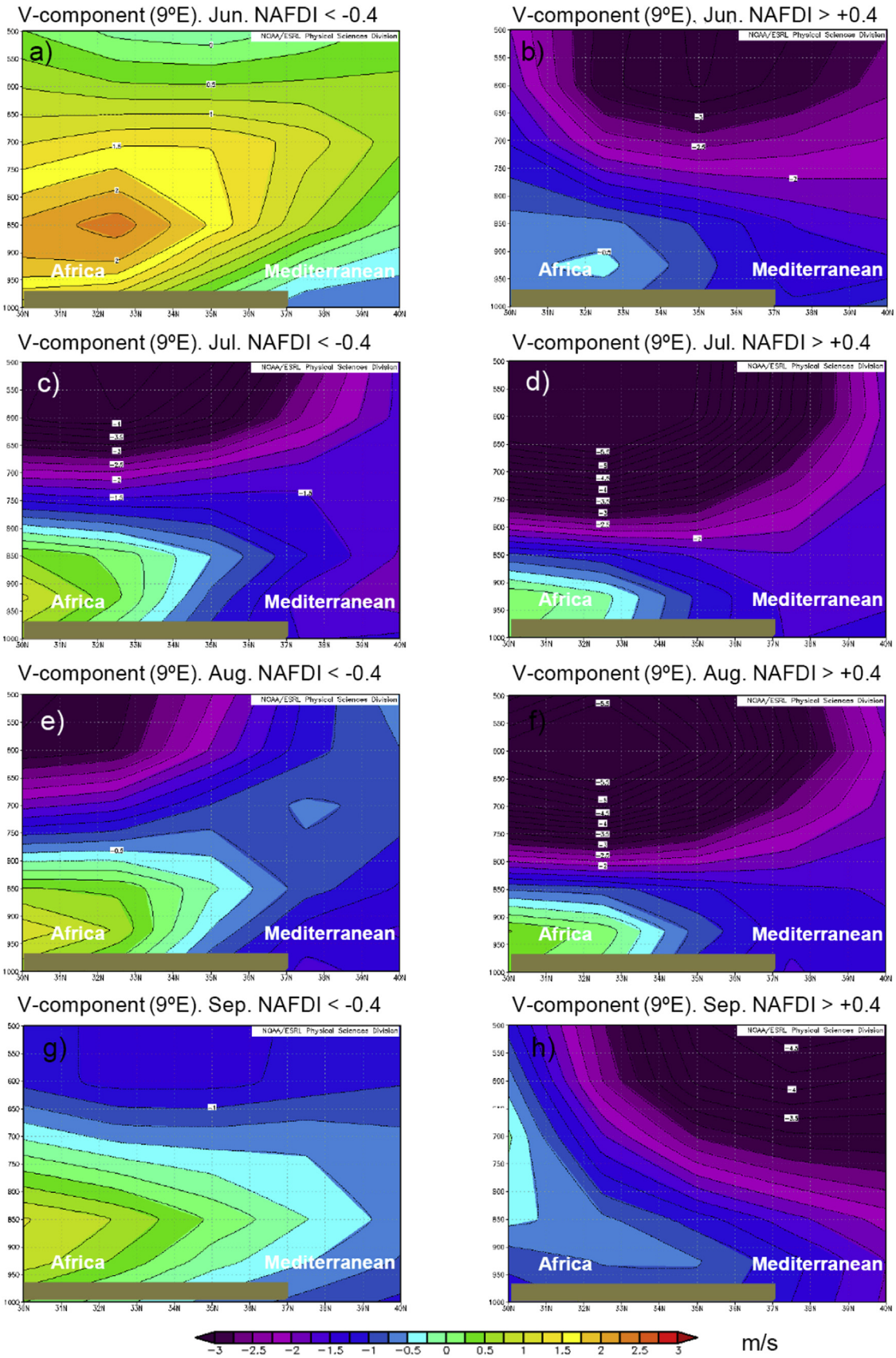

Fig. 5. Mean-meridional-wind-component (m s-1) latitude-height cross-sections along 9°E (Northern Africa and CWM) for June, July, August, and September months with negative (a, c, e, and g) and positive (b, d, f, and h) NAFDI (2003–2012) from NCEP/NCAR reanalysis.

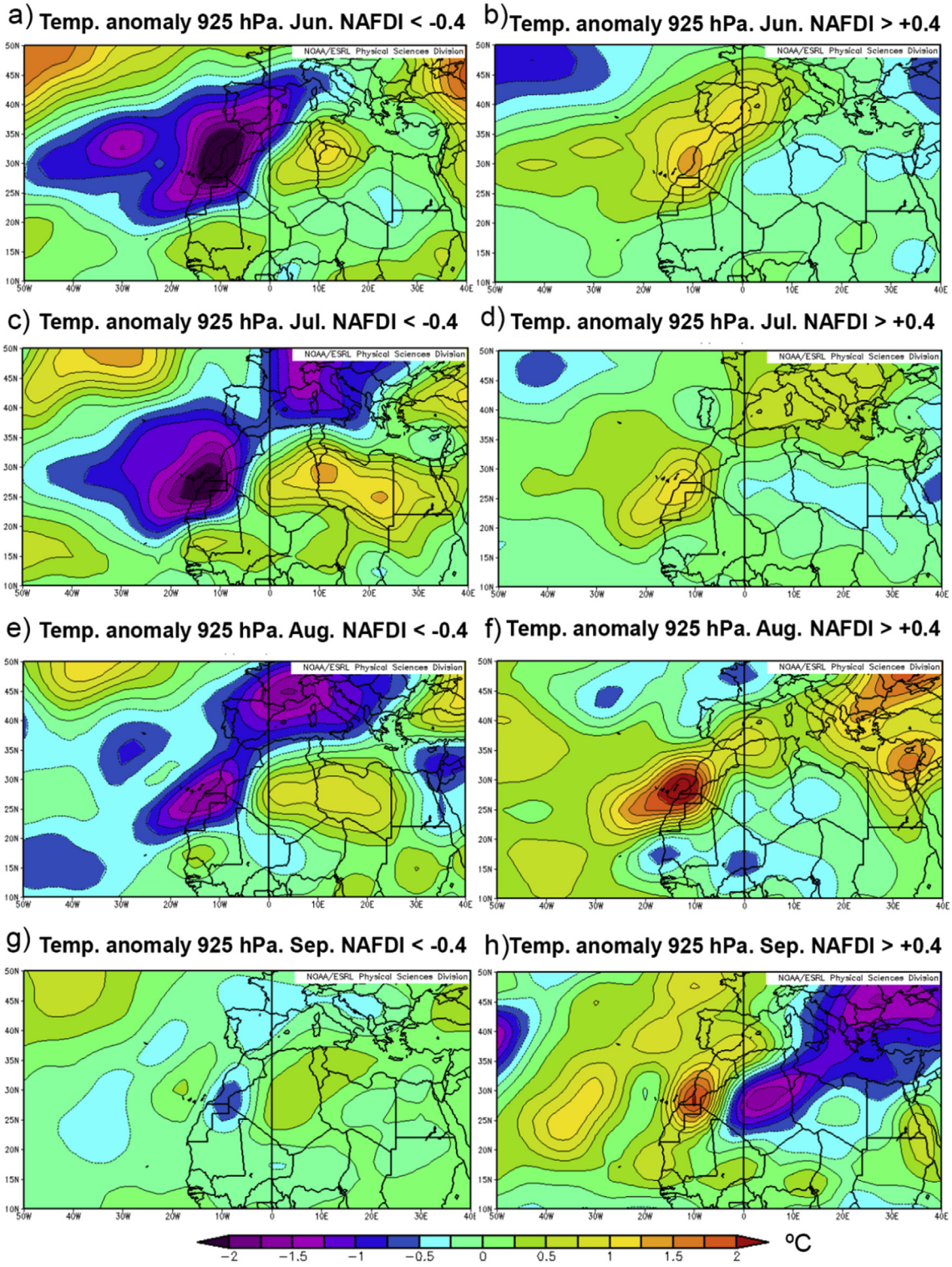

Fig. 6. Mean 925-hPa temperature anomaly (K) for June, July, August, and September months with negative (a, c, e, and g) and positive (b, d, f, and h) NAFDI (2003–2012) from NCEP/NCAR reanalysis.

Firstly, we compute a NAFDI daily index we call NAFDIDI for the 20 Jun. - 17 Sept. period using the NCEP reanalysis for the years 1980–2013. This period corresponds to the SHL period when the WAHL is located above the Sahara desert, according to Lavaysse et al. (2009). The daily index NAFDIDI is calculated as follows:

$$NAFDIDI = \frac{1}{10}((\Phi_{Mo} - <\Phi>_{Mo}) - (\Phi_{Ni} - <\Phi>_{Ni})) \quad (1)$$

where,

- Φ is the NCEP/NCAR daily average Z700 (m) for the considered day, at 5°W, 30°N (central Morocco) when the sub-index *Mo* is used, and at 5°E, 12.5°N (north Nigeria) when the sub-index *Ni* is used.
- < > denotes mean of the geopotential height (m) for the corresponding day of the year throughout 1981–2010 (reference period), and then applying a 29-day running average to the mean, for smoothing out the aleatory residuals.

It has also been introduced the daily SHL Longitudinal Shift Index (SHLLSI) as:

$$SHLLSI = \sum_n \frac{w_n}{3}[(T_{Wn} - <T_{Wn}>) - (T_{En} - <T_{En}>)] \quad (2)$$

where T_{Wn} is the air temperature (K) at the pressure level n, 12.5°W and 25°N, T_{En} is the air temperature (K) at the level n, 7.5°E and 20°N, and the operator < > has been defined in the previous paragraph (now applying on temperature instead of geopotential height). Those coordinates were chosen employing the locus of the minimum and maximum of the dipolar pattern corresponding to the SHL-location eigenvector shown in Fig. 5c of Lavaysse et al. (2013). The pressure levels n at which the summation is performed are 925, 850 and 700 hPa, in agreement with the pressure range 925–700 hPa used by Lavaysse et al. (2013) to identify the location of the SHL. The weights w_n are 0.5 for 925 hPa, 1.5 for 850 hPa, and 1 for 700 hPa, and were obtained integrating using the trapezoidal rule.

The close relationship between the daily SHLLSI and NAFDIDI for the 20 Jun.–17 Sept. 1980–2013 period (hereinafter denoted as 1980–2013 period) is shown in Fig. 7.

Fig. 7 also shows that the East-phase SHLLSI values (negative NAFDIDI) use to be greater in absolute value (and more infrequent) than the corresponding to the West-phase (positive NAFDIDI). The Pearson correlation coefficient (hereinafter, Pearson's r) between the daily SHLLSI and NAFDIDI is 0.70 (significant at the 99.999% level; see Supplement S6 for a description of the method used to compute confidence levels). We computed also the Pearson's r between the SHLLSI time series and the eigenvalue time series (shown in Fig. 6c of Lavaysse et al., 2013) associated to the mentioned EOF for the 2007–2011 period (for the same summer period as in the present paper), finding a r = −0.74. The negativity sign comes since Lavaysse et al. (2013) considered as positive the SHL East-phase.

We have explored the causality of the relationship between the NAFDIDI and the SHLLSI computing the Pearson's r with time-lag between them for the 1980–2013 period. Time-lag Pearson's r are shown in Table 1. The larger Pearson's r, 0.78 (significant at the 99.999% level), is obtained when the SHLLSI is 1-day lagged after the NAFDIDI. The correlation is even higher (0.864) if the one-day time-lagged correlation is performed after applying to both time series a 5-day running average. However, the Pearson's r is < 0.52 when NAFDIDI is lagged 1 day after the SHLLSI, which is actually lower than that obtained when the SHLLSI is lagged 3 days after the NAFDIDI (Table 1). There is a confidence level of 92.9% about the fact that the one-day lagged correlation is significantly larger than the no lagged correlation (the method used to compute confidence levels is described in Supplement S6). These results indicate that NAFDI changes occur before the displacement of the SHL.

Table 1
Time-lagged Pearson's r between the SHLLSI and NAFDIDI for the 1980–2013 period. "Time lag" (in days) means the SHLLSI lag behind the NAFDIDI.

Time lag	Pearson's r
−1	0.515
0	0.702
1	**0.783**
2	0.718
3	0.563

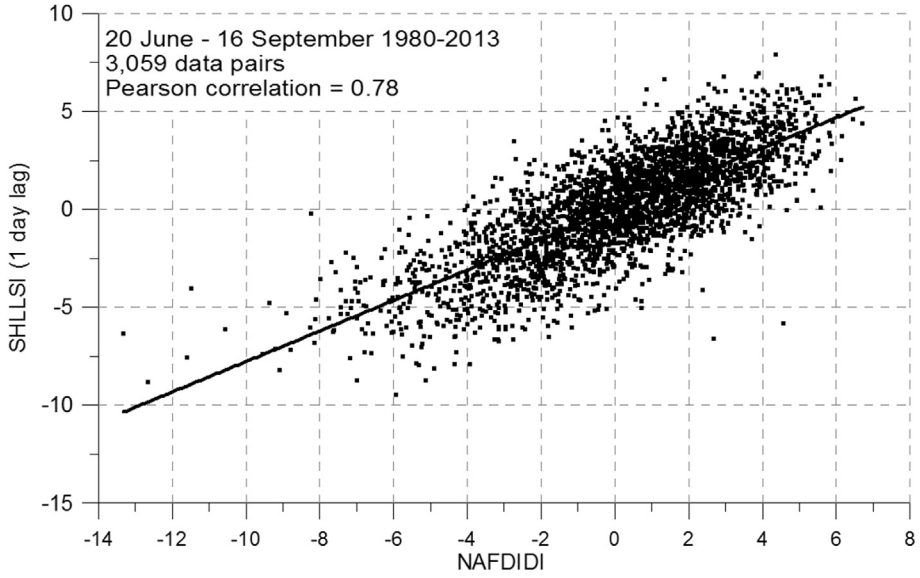

Fig. 7. NAFDIDI vs. SHLLSI one-day lagged for the summer period 1980–2013. The Pearson daily correlation value (0.78) is significant with a 99.999% confidence level.

The different monthly behaviour concerning dust transport in June and September compared with July and August, observed in Sect. 3.1, might be also caused by a combination of the following two facts: 1) the SHL is only present during 10 days of June and 17 days of September; and 2) the SHL is located in a more south-eastern position during June and September (e.g., Fig. 4 of Lavaysse et al., 2009).

3.2.2. Physical mechanics by which NAFDI drives the SHL longitudinal shifts

In this sub-section we show, using the energy equation of the atmospheric dynamics and the NCEP/NCAR reanalysis, that NAFDI drives SHL longitudinal displacements through horizontal advection of temperature. The energy equation in pressure coordinates (e.g., Holton, 1992) is:

$$\frac{\partial T}{\partial t} = -\boldsymbol{v}\cdot\nabla_p T - \omega T\frac{\partial \ln\theta}{\partial p} + \frac{J}{c_p}, \tag{3}$$

where $\boldsymbol{v}$ is the horizontal velocity, p is the pressure, θ is the potential temperature, ω is the vertical velocity in pressure coordinates, J is the diabatic heating per mass unit, and c_p is the specific heat at constant pressure. This equation indicates that the variation in time of the temperature at a fixed Eulerian grid point is due to the horizontal advection of temperature, the temperature tendency due to omega and the diabatic heating. Note that the temperature tendency due to omega indeed contains the vertical advection of temperature and the adiabatic heating associated to the pressure changes.

Combining Eqs. (2) and (3), the following equation for the time evolution of the SHLLSI is obtained, which involves variables and gradients at the two geographical points used to define the SHLLSI denoted with the sub-indexes W and E and the three pressure levels n (925, 850 and 700 hPa):

$$\frac{\partial SHLLSI}{\partial t} = HAdv + Ome + Diab - \sum_n \frac{w_n}{3}\frac{\partial(<T_{Wn}> - <T_{En}>)}{\partial t}, \tag{4}$$

where

$$HAdv = \sum_n \frac{w_n}{3}\left(-\boldsymbol{v_{Wn}}\cdot\nabla_p T_{Wn} + \boldsymbol{v_{En}}\cdot\nabla_p T_{En}\right), \tag{5}$$

and

$$Ome = \sum_n \frac{w_n}{3}\left(-\omega_{Wn}T_{Wn}\frac{\partial \ln\theta_{Wn}}{\partial p} + \omega_{En}T_{En}\frac{\partial \ln\theta_{En}}{\partial p}\right), \tag{6}$$

$$Diab = \sum_n \frac{w_n}{3}\left(\frac{J_{Wn} - J_{En}}{c_p}\right). \tag{7}$$

Equation (4) indicates that the variation in time of the SHLLSI is due to the differential, West minus East, horizontal advection of temperature (*HAdv*), the differential temperature tendency due to omega (*Ome*), the differential diabatic heating (*Diab*), and the variation in time of the climatological reference temperatures used in the SHLLSI definition (see Eq. (2)).

We have computed each of the terms in Eq. (4) at 6-hourly timescale for the 1980–2013 period and thereafter obtained daily averages (see details in Supplement S7). The contribution of the last term of Eq. (4) is negligible. We have computed the mean anomaly of each term of the Eq. (4), for different regions of the "phase space" delimited by the tertiles of SHLLSI and the quartiles of its time derivative (Table 2). Tertiles are appropriate for SHLLSI since they split the phase space in (significant) East, neutral and West phases, however for its time derivative we use quartiles since they allow distinguish between strong change rates (extreme quartiles) and weak change rates (central quartiles), which we consider as representative of states of quasi-equilibrium. Extreme quartiles are considered as indicative of transitions between phases when the phase is neutral, and as indicative of building or decreasing of a phase when the phase is not neutral. Table 2 follows this nomenclature and avoids indicating explicitly the tertiles and quartiles for easiness of reading and interpretation.

Table 2
Mean anomaly of the terms of Eq. (4) for different regions of the "phase space" with axes SHLLSI and its time derivative (see the main text of the paper).

Stage	*HAdv* (K/day)	*Ome* (K/day)	*Diab* (K/day)
Transition from East to West	1.08	0.04	0.81
Building West	2.30	−0.89	0.50
West Equilibrium	1.50	−1.26	−0.21
Decreasing West	0.50	−1.47	−0.91
Transition from West to East	−1.12	−0.40	−0.45
Building East	−3.06	1.51	−0.60
East Equilibrium	−1.47	1.47	0.02
Decreasing East	0.03	1.43	0.57
Neutral equilibrium	0.31	−0.48	0.13

The differential horizontal advection of temperature (*HAdv*) drives the departure of SHLLSI from its neutral position ("Building" stages in Table 2). Quasi-stationary extreme SHLLSI phases ("Equilibrium" stages in Table 2) are possible due to the building up of a negative feedback (mainly in *Ome*) that tends to restore SHLLSI to its neutral phase. Once the driver starts to diminish, the negative feedback restores SHLLSI to its neutral position ("Decreasing" stages in Table 2). This interpretation is also supported by the statistics presented below.

We define the "driving stage" as the time periods in which SHLLSI >0 and its time derivative is in the 4th quartile, or SHLLSI<0 and its time derivative is in the 1st quartile. On the other hand, we define the "restoring stage" as the time period in which SHLLSI<0 and its time derivative is in the 4th quartile, or SHLLSI>0 and its time derivative is in the 1st quartile. During the "driving stage" the daily Pearson correlation between the time derivative of SHLLSI and HAdv is 0.740 (significant at the 99.999% level), while the correlation between SHLLSI and (Diab + Ome) is −0.072 (not significant). On the contrary, during the "restoring stage", the daily Pearson correlation between the time derivative of SHLLSI and (Diab + Ome) is 0.647 (significant at the 99.97% level), while the correlation between SHLLSI and HAdv is 0.160 (not significant).

Now the question is, what drives HAdv? Below it is shown that the answer is the NAFDI. The daily Pearson correlation between NAFDIDI and: a) *HAdv* is 0.612 (0.767 under the "driving stage"; both correlations are significant at the 99.999% level), b) (*Ome* + *Diab*) is −0.471 (significant at the 99.999% level). This suggests that *HAdv* is driven by the daily horizontal velocity anomaly associated to NAFDI, which has been obtained by fitting the daily velocity as a linear function of NAFDIDI, for the full period considered. Note that, in essence, NAFDI is a large-scale geostrophic wind anomaly. In order to confirm this hypothesis, we have computed a *synthetic HAdv* using the daily wind anomaly associated to NAFDIDI and the mean climatological temperature gradient. The daily correlation between *HAdv* and this *synthetic HAdv* is 0.767 under the "driving stage". This indicates that NAFDI drives the time variation of the SHL longitudinal shift through horizontal advection of temperature. Moreover, the daily correlation between NAFDIDI and the time derivative of SHLLSI is 0.770 under the "driving stage" (for all the stages: 0.260, which is significant at the 99.8% level). Finally, the daily correlation between SHLLSI and its time derivative

during the "restoring stage" is −0.745 (0.000 for all the stages), which is significant at the 99.999% level and supports the existence of the negative feedback that tends to restore SHLLSI to its "neutral stage".

3.2.3. Possible impact on dust sources activation over the CWS

Saharan dust sources are basically found in the many interior drainage basins that exist in this vast desert (Ginoux et al., 2012; Middleton and Goudie, 2001; Prospero et al., 2002; Schepanski et al., 2007). Dust sources in the Sahara are principally triggered by LLJs associated to the Harmattan wind and the West African Monsoon wind field (Allen and Washington, 2013; Conway and John, 2014), which are modulated somehow by intensity changes and longitudinal shift of the SHL (e.g. Couvreux et al., 2010; Lavaysse et al., 2010a,b), and the latter, in turn, by variations of NAFDI.

The MODIS AOD anomaly fields show that, a substantial increase of dust over the western-most part of the CWS is observed under positive NAFDI (SHL West-phase; see Fig. 1), while the opposite occurs with negative NAFDI. However, from only AOD data it is not possible to differentiate between dust emitted locally and dust advected from other source regions.

Considering the above, and as a preliminary approach, we have calculated dust emissions in order to ascertain whether NAFDI and SHL-phase changes exert a potential impact on intensification or abatement of dust sources in different regions of the Sahara at large scale. Following a relatively simple approach for the dust emission estimation (e.g., Gillette and Passi, 1988; Morcrette et al., 2009; Tegen and Fung, 1994), we have computed the instantaneous emission (E) at the hours 00, 06, 12 and 18 GMT, using the following equation:

$$E = SV_{10}^2(V_{10} - V_T) \quad (8)$$

where S is the dust emission potential (Morcrette et al., 2009), V_{10} is the wind velocity at 10-m height, and V_T is a dust-raise threshold wind velocity set to be 6.5 ms^{-1} (Helgren and Prospero, 1987; Takemura et al., 2000), obtained from MACC reanalysis. Then, we have computed averages for each summer month and each phase of NAFDI. The dust emission patterns agree (Fig. 8) quite well with the multi-model mean June–September dust emission distribution from 14 global models contributing to the fifth Coupled Model Intercomparison Project (Todd and Cavazos-Guerra, 2016).

The main differences in dust emissions over the CWS between the positive and negative NAFDI phases for each month are described below. In June, for negative NAFDI (Fig. 8a), there is an increase in Chotts el Jerïd and Melrhir (northeast of Algeria and Tunisia) marked as region 1 in Fig. 8), which are known relevant dust sources (Ginoux et al., 2012; Rodríguez et al., 2011). This is consistent with the abundant dust outflow towards the Mediterranean Sea for this month under negative NAFDI (Fig. 1a). There is a notable activation of the Grand-Erg Occidental dust source, identified by Ginoux et al. (2012), during positive NAFDI for all months (region 2; Fig. 8). This agrees with significant dust mobilization under positive NAFDI in the so-called Subtropical Saharan Stripe region (Rodríguez et al., 2015). Quite similar emissions in the Tiris Zemmour region (Western Sahara; region 3, Fig. 8) during both NAFDI phases are observed.

The CWS was the object of a detailed dust-source study carried out by Ashpole and Washington (2013) in two specific regions: the TP (Algeria-Mali-Niger triple-point border) and the MAB (northern Mali-Algeria border), both marked in Fig. 8. They observed that the SHL is more frequently found over central and southern Algeria (SHL East-Phase) when dust appears in the proximities of the TP, while when dust is predominantly in the MAB, the SHL is normally found over northern Mauritania, northwest Mali, and western-most Algeria (SHL West-phase). The averaged emissions we have computed clearly agree with Ashpole and Washington (2013) in the MBA case, whilst for the TP region the agreement is not so clear. Most likely, MACC underestimates dust emissions in TP because most of the dust raised on this region in summertime is caused by mesoscale convective systems, as reported by Marticorena et al. (2010), which MACC cannot reproduce well (Cuevas et al., 2015).

These preliminary rough estimates on dust emissions suggest that changes in NAFDI might be also related with the intensification/weakening of dust sources in the CWS. However, further accurate analysis using more complex high-resolution dust emission modelling are needed to confirm these results. Similar to these results in the Sahara, Kaskaoutis et al. (2017) found with model simulations that high CasHKI modes are associated with higher dust emissions and concentrations over the South West Asia.

3.3. Connection between mid-latitude Rossby waves and NAFDI

Using NCEP2 reanalysis, Chauvin et al. (2010) carried out EOF analyses to the potential-temperature field at 850 hPa over a North African region. They observed that the arrival to southwest Europe and northwest Africa of MLRWs propagating along the North-Atlantic-North-African waveguide drives, someway, the SHL phases. Here we show that the intra-seasonal geopotential height variations at synoptic scales associated to NAFDI seem to be indeed the changing lower-level state imposed by the MLRWs propagating along the upper troposphere. We have already mentioned in Sect. 3.1 that the Z700 pattern associated to NAFDI is also present at the pressure levels 850, 500 and 200 hPa (see Supplement S3), and even vaguely at 1000 hPa. That result was based on monthly correlations. In this section, we consider daily data.

Geisler and Dickinson (1975) computed Rossby modes considering an atmospheric background state having an empirical variation of the zonal wind with altitude. In Supplement S8 we show that: 1) the vertical variation of the background wind allows the MLRB having a quite prominent amplitude in the low and mid-troposphere; and 2) there is an empirical relationship, over the region of interest, between the 500-hPa Omega amplitude and the variation in altitude of the background flow using NCEP/NCAR reanalysis data. These results seem to indicate that the impact of a MLRB in the lower levels depends on its ability to penetrate into the low-troposphere additionally to on its amplitude in the upper portion of the troposphere. The former can be quantified using Omega at 500 hPa.

Taking into account those results, we employ the daily NCEP 500-hPa Omega (Pa/s) to quantify the entry of the MLRB into the low-troposphere over North Africa, and denote it as OM500. The selected geographical location over Northern Algeria (32.5° N, 2.5° E) was chosen because the correlation between the NAFDI and the 500-hPa omega field presents, for the 1980–2013 August months, a relative maximum (~0.6). A very similar behaviour is observed for the full June–September period (see Supplement S9). We chose the 500-hPa level due to the fact that it is an intermediate level and therefore the wind shear at this level might represent approximately the mean corresponding to the full troposphere, and it is not sensitive to the unwanted SHL-feedback. The hypothetical impact of the Saharan CBL in OM500 is ruled out because: 1) The maximum monthly mean CBL height at this point, from ECMWF reanalysis, is observed in July, being 4664 ± 297 (1 standard deviation) m under negative NAFDI and 4510 ± 198 m under positive NAFDI; and 2) the monthly NCEP regression (Pa/s/NAFDI) and correlation plots between NAFDI and upper-level (300, 400 and 500 hPa) omega fields for 1980–2013 June–September months show quite similar patterns (see Supplement S9), and it is very clear

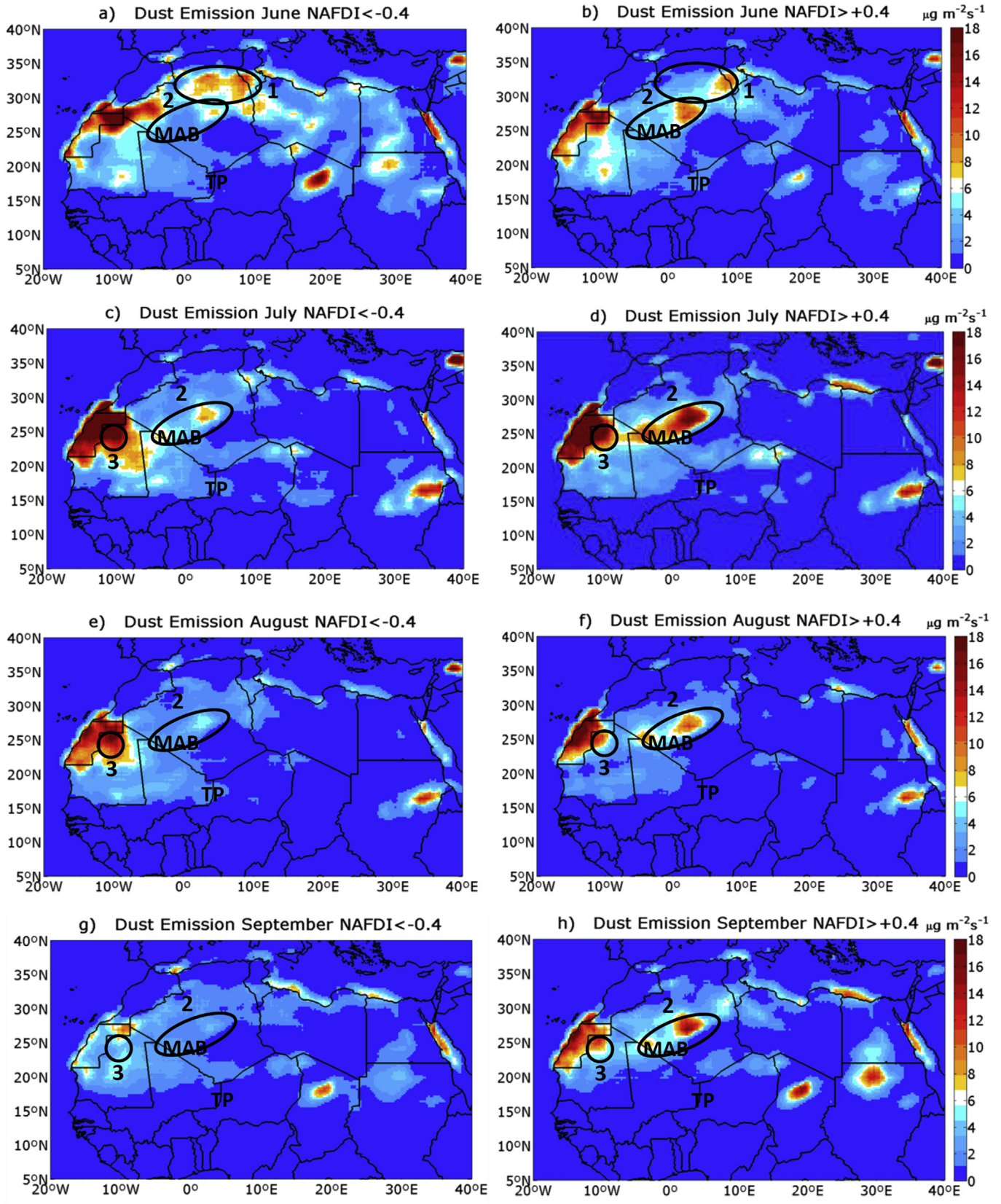

Fig. 8. Mean dust emission (μg $m^{-2}s^{-1}$) calculated from MACC reanalysis for June, July, August, and September months with negative (a, c, e, and g) and positive (b, d, f, and h) NAFDI (2003–2012).

that the 300 and 400 hPa levels are not affected at all by the Saharan CBL. On the contrary, the corresponding correlation pattern at 600 hPa is shifted to the south, which might be a sign of the Saharan CBL impact at this lower level.

We employ the NCEP daily 300-hPa zonal Wind Anomaly (m/s) with its sign inverted, and denote it as WA300, to quantify approximately the phase and amplitude of the MLRW at this level over North Africa. The selected geographical location in South Morocco (10° W; 30° N) corresponds to a maximum negative correlation (<- 0.8) at the upper levels between the NAFDI for August months and the zonal wind (similar results hold for the entire summer period as shown in Supplement S9). Note that we have calculated the anomaly with respect to the daily climatology smoothed by a 29-day running mean, as for the daily SHLLSI and NAFDIDI computations, and therefore we have ruled out climatological changes in the zonal wind of the waveguide. We have also computed the vertical profile of the Rossby wave amplitude (see Supplement S8) and found that it is very similar to that corresponding to one of the external modes that Geisler and Dickinson (1975) obtained.

After smoothing the time series using 5-day running average, the correlation between the NAFDIDI and a linear combination of WA300 and OM500 is 0.656 (significant at the 99.999% level). The mentioned linear combination was obtained carrying out a least-square regression of NAFDIDI as a linear polynomial of WA300 and OM500. These results point out that WA300 and OM500 are quasi-independent (the correlation between them is 0.105, being 0.205 if a 5-day running average is previously used) that account for different features of the MLRB, as discussed previously.

The power spectra of the NAFDIDI, SHLLSI, and LCWAOM (the linear combination of WA300 and OM500 time series mentioned in the previous paragraph) time series for the period 1980–2013 have been computed using Fast Fourier Transform, being the overall structure of all those spectra considerably similar. The power spectrum for NAFDIDI for the intermediate time-scale domain (10–30 days), which is the MLRW temporal domain (e.g., Ambrizzi et al., 1995), shows that the majority of the strong peaks are present too in the SHLLSI spectrum, finding that a lot of them correspond as well to LCWAOM peaks (see Supplement S10). These results indicate that NAFDI seems to quantify the intra-seasonal changes in the lower-level intensity of those MLRWs that penetrate deep enough to impose their perturbation to the lower-troposphere background meteorological fields over Northern Africa. These intra-seasonal changes seem to explain the pulsating nature of the Saharan-dust large-scale export out of Northern Africa.

4. Conclusions

The main conclusions of this study are as follows:

1 We have complemented the findings of Rodríguez et al. (2015). They reported an inter-annual variation (only August months were studied) in dust outflows towards the Subtropical Atlantic associated to the variations of NAFDI. In this paper we have shown that NAFDI also presents a notable intra-seasonal variation. Moreover, for each phase of the NAFDI, specific large scale patterns of AOD anomalies over the SNA, the Mediterranean basin, and the interior of North Africa are found during the summer period, depending only weakly on the specific summer month. This suggests that NAFDI modulates dust outflows towards the SNA and the Mediterranean into alternate phasing. Moreover, under positive NAFDI, positive AOD anomalies are observed in the Western Sahara and SNA, while during negative NAFDI they are found in central-eastern Sahara and CWM regions.

2 For the first time, it has been shown there is a close relationship between SHL West (East) phase and positive (negative) NAFDI. The Pearson's r between the newly introduced daily SHLLSI and NAFDIDI data series for the period between late June and mid-September (1980–2013) is 0.70. This correlation increases to 0.78 when the SHLLSI is 1-day lagged behind NAFDIDI.

3 Using the energy equation of the atmospheric dynamics and the NCEP/NCAR reanalysis, we have shown that the differential horizontal advection of temperature, which is in turn due to the daily horizontal velocity anomaly associated to NAFDI, drives the temporal evolution of the longitudinal displacement of the SHL.

4 Preliminary estimates on dust emissions from MACC reanalysis suggest that changes in NAFDI may be related with the intensification/weakening of dust sources in CWS. Specifically, positive NAFDI seems to favour dust mobilization in Western Sahara, northern Mauritania, and central Algeria.

5 NAFDI intra-seasonal variations are driven by those MLRWs propagating over North Africa that penetrate sufficiently into the lower troposphere. A multi-linear least square regression model has been built to describe the NAFDI as a function of WA300, which quantifies the wave amplitude and phase at 300 hPa, and OM500, which quantifies the wave penetration into the lower troposphere. It presents a linear correlation of 0.656.

Summarizing, the results of this study indicate that the NAFDI intra-seasonal variations are driven by those MLRWs that impose their perturbation to the lower-troposphere over Northern Africa, and that NAFDI drives, in turn, the SHL West-East displacements, the pulsed transport of Saharan-dust over the SNA and the Mediterranean basin, and the spatial and intensity intra-seasonal changes in dust mobilization over the Sahara.

The analysis of the processes that drive the inter-annual variations of NAFDI is beyond the scope of the present paper, and is the subject of an on-going study.

Acknowledgements

This work is part of the research activities developed by the WMO SDS-WAS Regional Centre for Northern Africa, Middle East and Europe, held by AEMET and BSC-CNS. This study also contributes to Copernicus Atmosphere Monitoring Service (CAMS). Our acknowledgment to ECMWF for providing MACC-dust reanalysis. The authors wish to thank NCEP/NCAR Reanalysis Project. We acknowledge NASA LADS for providing MODIS data. The University of Granada (Spain) and its “Physics and Space Sciences” PhD Programme are acknowledged by A. J. Gómez-Peláez and E. Cuevas. AEROATLAN project (CGL2015-17 66229-P), co-funded by the Ministry of Economy and Competitiveness of Spain and the European Regional Development Fund contributed to this study. Sara Basart acknowledges the CICYT project (CGL2013-46736).

Appendix A. Supplementary data

Supplementary data related to this article can be found at http://dx.doi.org/10.1016/j.atmosenv.2017.08.059.

References

Adams, A.M., Prospero, J.M., Zhang, C., 2012. CALIPSO derived three-dimensional structure of aerosol over the Atlantic Basin and adjacent continents. J. Clim. 25, 6862–6879. http://dx.doi.org/10.1175/JCLI-D-11-00672.1.

Allen, C.J.T., Washington, R., 2013. The low-level jet dust emission mechanism in the central Sahara: observations from Bordj-Badji Mokhtar during the June 2011 fennec intensive observation period. J. Geophys. Res. Atmos. 119, 2990–3015.

http://dx.doi.org/10.1002/2013JD020594.
Ambrizzi, T., Hoskins, B.J., Hsu, H.H., 1995. Rossby-wave propagation and teleconnection patterns in the austral winter. J. Atmos. Sci. 52, 3661–3672.
Ashpole, I., Washington, R., 2013. Intraseasonal variability and atmospheric controls on daily dust occurrence frequency over the central and Western Sahara during the boreal summer. J. Geophys. Res.-Atmos 118, 12915–12926. http://dx.doi.org/10.1002/2013JD020267.
Barnaba, F., Gobbi, G.P., 2004. Aerosol seasonal variability over the Mediterranean region and relative impact of maritime, continental and Saharan dust particles over the basin from MODIS data in the year 2001. Atmos. Chem. Phys. 4, 2367–2391. http://dx.doi.org/10.5194/acp-4-2367-2004.
Basart, S., Pérez, C., Cuevas, E., Baldasano, J.M., Gobbi, G.P., 2009. Aerosol characterization in Northern Africa, Northeastern Atlantic, Mediterranean basin and Middle East from direct-sun AERONET observations. Atmos. Chem. Phys. 9, 8265–8282.
Bellouin, N., Quaas, J., Morcrette, J.-J., Boucher, O., 2013. Estimates of aerosol radiative forcing from the MACC re-analysis. Atmos. Chem. Phys. 13, 2045–2062. http://dx.doi.org/10.5194/acp-13-2045-2013.
Ben-Ami, Y., Koren, I., Altaratz, O., 2009. Patterns of North African dust transport over the Atlantic: winter vs. summer, based on CALIPSO first year data. Atmos. Chem. Phys. 9, 7867–7875. http://dx.doi.org/10.5194/acp-9-7867-2009.
Benedetti, A., Morcrette, J.-J., Boucher, O., Dethof, A., Engelen, R.J., Fisher, M., Flentjes, H., Huneeus, N., Jones, L., Kaiser, J.W., Kinne, S., Mangold, A., Razinger, M., Simmons, A.J., Suttie, M., the GEMS-AER team, 2009. Aerosol analysis and forecast in the ECMWF integrated forecast system. Part II: data assimilation. J. Geophys. Res. 114, D13205. http://dx.doi.org/10.1029/2008JD011115.
Benedetti, A., Baldasano, J.M., Basart, S., Benincasa, F., Boucher, O., Brooks, M., Chen, J.-P., Colarco, P.R., Gong, S., Huneeus, N., Jones, L., Lu, S., Menut, L., Morcrette, J.-J., Mulcahy, J., Nickovic, S., Pérez, C., Reid, J.S., Sekiyama, T.T., Tanaka, T.Y., Terradellas, E., Westphal, D.L., Zhang, X.-Y., Zhou, C.-H., 2014. Numerical prediction of dust. In: Knippertz, P., Stuut, J.-B. (Eds.), Mineral Dust – a Key Player in the Earth System. Springer, Dordrecht, pp. 230–240.
Cesnulyte, V., Lindfors, A.V., Pitkänen, M.R.A., Lehtinen, K.E.J., Morcrette, J.-J., Arola, A., 2014. Comparing ECMWF AOD with AERONET observations at visible and UV wavelengths. Atmos. Chem. Phys. 14, 593–608. http://dx.doi.org/10.5194/acp-14-593-2014.
Chauvin, F., Roehrig, R., Lafore, J.-P., 2010. Intraseasonal variability of the Saharan heat low and its link with midlatitudes. J. Clim. 23, 2544–2561. http://dx.doi.org/10.1175/2010JCLI3093.1.
Chiapello, I., Moulin, C., Prospero, J.M., 2005. Understanding the long-term variability of African dust transport across the Atlantic as recorded in both Barbados surface concentrations and large-scale Total Ozone Mapping Spectrometer (TOMS) optical thickness. J. Geophys. Res. 110, D18S10. http://dx.doi.org/10.1029/2004JD005132.
Conway, T.M., John, S.G., 2014. Quantification of dissolved iron sources to the North Atlantic Ocean. Nature 511, 212–215. http://dx.doi.org/10.1038/nature13482.
Couvreux, F., Guichard, F., Bock, O., Campistron, B., Lafore, J.-P., Redelsperger, J.-L., 2010. Synoptic variability of the monsoon flux over West Africa prior to the onset. Q. J. R. Meteorol. Soc. 136 (S1), 159–173. http://dx.doi.org/10.1002/qj.473.
Cuesta, J., Marsham, J.H., Parker, D.J., Flamant, C., 2009. Dynamical mechanisms controlling the vertical redistribution of dust and the thermodynamic structure of the West Saharan atmospheric boundary layer during summer. Atmos. Sci. Lett. 10, 34–42. http://dx.doi.org/10.1002/asl.207.
Cuevas, E., Camino, C., Benedetti, A., Basart, S., Terradellas, E., Baldasano, J.M., Morcrette, J.J., Marticorena, B., Goloub, P., Mortier, A., Berjón, A., Hernández, Y., Gil-Ojeda, M., Schulz, M., 2015. The MACC-II 2007–2008 reanalysis: atmospheric dust evaluation and characterization over northern Africa and the Middle East. Atmos. Chem. Phys. 15, 3991–4024. http://dx.doi.org/10.5194/acp-15-3991-2015.
Díaz, J., Tobías, A., Linares, C., 2012. Saharan dust and association between particulate matter and case-specific mortality: a casecrossover analysis in Madrid (Spain). Environ. Health 11, 1–6. http://dx.doi.org/10.1186/1476-069X-11-11.
Engelstaedter, S., Washington, R., 2007. Atmospheric controls on the annual cycle of North African dust. J. Geophys. Res. 112, D17111. http://dx.doi.org/10.1029/2006JD007195.
Engelstaedter, S., Washington, R., Mahowald, N., 2009. Impact of changes in atmospheric conditions in modulating summer dust concentration at Barbados: a back-trajectory analysis. J. Geophys. Res. 114, D17111. http://dx.doi.org/10.1029/2008JD011180.
Engelstaedter, S., Washington, R., Flamant, C., Parker, D.J., Allen, C.J.T., Todd, M.C., 2015. The Saharan heat low and moisture transport pathways in the central Sahara—multiaircraft observations and Africa-LAM evaluation. J. Geophys. Res. 120 (10), 4417–4442. http://dx.doi.org/10.1002/2015JD023123.
Escudero, M., Querol, X., Ávila, A., Cuevas, E., 2007. Origin of the exceedances of the European daily PM limit value in regional background áreas of Spain. Atmos. Environ. 41, 730–744.
Eskes, H., Huijnen, V., Arola, A., Benedictow, A., Blechschmidt, A.-M., Botek, E., Boucher, O., Bouarar, I., Chabrillat, S., Cuevas, E., Engelen, R., Flentje, H., Gaudel, A., Griesfeller, J., Jones, L., Kapsomenakis, J., Katragkou, E., Kinne, S., Langerock, B., Razinger, M., Richter, A., Schultz, M., Schulz, M., Sudarchikova, N., Thouret, V., Vrekoussis, M., Wagner, A., Zerefos, C., 2015. Validation of reactive gases and aerosols in the MACC global analysis and forecast system. Geosci. Model Dev. 8, 3523–3543. http://dx.doi.org/10.5194/gmd-8-3523-2015.
Evan, A.T., Flamant, C., Gaetani, M., Guichard, F., 2016. The past, present and future of African dust. Nature 531 (7595), 493–495.
Foltz, G.R., McPhaden, M.J., 2008. Impact of Saharan dust on tropical North Atlantic SST. J. Clim. 21, 5048–5060.
Gallisai, R., Peters, F., Volpe, G., Basart, S., Baldasano, J.M., 2014. Saharan dust deposition may affect phytoplankton growth in the Mediterranean Sea at ecological time scales. PloS one 9 (10), e110762.
Geisler, J.E., Dickinson, R.E., 1975. External Rossby modes on a beta-plane with realistic vertical wind shear. J. Atmos. Sci. 32, 2082–2093.
Gillette, D.A., Passi, R., 1988. Modeling dust emission caused by wind erosion. J. Geophys. Res.93 D11, 14233–14242. http://dx.doi.org/10.1029/JD093iD11p14233.
Ginoux, P., Prospero, J.M., Torres, O., Chin, M., 2004. Long-term simulation of global dust distribution with the GOCART model: correlation with North Atlantic Oscillation. Environ. Modell. Softw. 19, 113–128.
Ginoux, P., Prospero, J.M., Gill, T.E., Hsu, N.C., Zhao, M., 2012. Global-scale attribution of anthropogenic and natural dust sources and their emission rates based on MODIS Deep Blue aerosol products. Rev. Geophys 50, RG3005. http://dx.doi.org/10.1029/2012RG000388.
Gkikas, A., Houssos, E.E., Lolis, C.J., Bartzokas, A., Mihalopoulos, N., Hatzianastassiou, N., 2015. Atmospheric circulation evolution related to desert dust episodes over the Mediterranean. Q. J. R. Meteorol. Soc. 141 (690), 1634–1645.
Gläser, G., Wernli, H., Kerkweg, A., Teubler, F., 2015. The transatlantic dust transport from North Africa to the Americas—its characteristics and source regions. J. Geophys. Res. Atmos. 120, 11,231–11,252. http://dx.doi.org/10.1002/2015JD023792.
Goudie, A.S., Middleton, N.J., 2001. Saharan dust storms: nature and consequences. Earth Sci. Rev. 56 (1), 179–204.
Guerzoni, S., Chester, R., Dulac, F., Herut, B., Loye-Pilot, M.-D., Measures, C., Migon, C., Molinaroli, E., Moulin, C., Rossini, P., Saydam, C., Soudine, A., Ziveri, P., 1999. The role of atmospheric deposition in the biogeochemistry of the Mediterranean Sea. Prog. Oceanogr. 44, 147–190.
Helgren, D.M., Prospero, J.M., 1987. Wind velocities associated with dust deflation events in the Western Sahara. J. Clim. Appl. Meteorol. 26, 1147–1151.
Holton, J.R., 1992. An Introduction to Dynamic Meteorology, Third Edition, International Geophysics Series, vol. 48. Academic Press, San Diego, California.
Huneeus, N., Schulz, M., Balkanski, Y., Griesfeller, J., Prospero, J., Kinne, S., Bauer, S., Boucher, O., Chin, M., Dentener, F., Diehl, T., Easter, R., Fillmore, D., Ghan, S., Ginoux, P., Grini, A., Horowitz, L., Koch, D., Krol, M.C., Landing, W., Liu, X., Mahowald, N., Miller, R., Morcrette, J.-J., Myhre, G., Penner, J., Perlwitz, J., Stier, P., Takemura, T., Zender, C.S., 2011. Global dust model intercomparison in AeroCom phase I. Atmos. Chem. Phys. 11, 7781–7816. http://dx.doi.org/10.5194/acp-11-7781-2011.
Huneeus, N., Boucher, O., Chevallier, F., 2013. Atmospheric inversion of SO2 and primary aerosol emissions for the year 2010. Atmos. Chem. Phys. 13, 6555–6573. http://dx.doi.org/10.5194/acp-13-6555-2013.
Inness, A., Baier, F., Benedetti, A., Bouarar, I., Chabrillat, S., Clark, H., Clerbaux, C., Coheur, P., Engelen, R.J., Errera, Q., Flemming, J., George, M., Granier, C., Hadji-Lazaro, J., Huijnen, V., Hurtmans, D., Jones, L., Kaiser, J.W., Kapsomenakis, J., Lefever, K., Leitão, J., Razinger, M., Richter, A., Schultz, M.G., Simmons, A.J., Suttie, M., Stein, O., Thépaut, J.-N., Thouret, V., Vrekoussis, M., Zerefos, C., the MACC team, 2013. The MACC reanalysis: an 8 yr data set of atmospheric composition. Atmos.Chem. Phys. 13, 4073–4109. http://dx.doi.org/10.5194/acp-13-4073-2013.
Israelevich, P., Ganor, E., Alpert, P., Kishcha, P., Stupp, A., 2012. Predominant transport paths of Saharan dust over the mediterranean sea to Europe. J. Geophys. Res. 117, D02205. http://dx.doi.org/10.1029/2011JD016482.
Kalnay, E., Kanamitsu, M., Kistler, R., Collins, W., Deaven, D., Gandin, L., Iredell, M., Saha, S., White, G., Woollen, J., Zhu, Y., Leetmaa, A., Reynolds, R., Chelliah, M., Ebisuzaki, W., Higgins, W., Janowiak, J., Mo, K.C., Ropelewski, C., Wang, J., Jenne, R., Joseph, D., 1996. The NCEP/NCAR 40-year reanalysis project. B. Am. Meteorol. Soc. 77, 437–471.
Karanasiou, A., Moreno, N., Moreno, T., Viana, M., de Leeuw, F., Querol, X., 2012. Health effects from Sahara dust episodes in Europe: literature review and research gaps. Environ. Int. 47, 107–114.
Kaskaoutis, D.G., Houssos, E.E., Rashki, A., Francois, P., Legrand, M., Goto, D., Bartzokas, A., Kambezidis, H.D., Takemura, T., 2016. The Caspian sea-hindu Kush index (CasHKI): a regulatory factor for dust activity over southwest Asia. Glob. Planet. Change 137, 10–23.
Kaskaoutis, D.G., Alireza, R., Houssos, E.E., Legrand, M., Francois, P., Bartzokas, A., Kambezidis, H.D., Dumka, U.C., Goto, D., Takemura, T., 2017. Assessment of changes in atmospheric dynamics and dust activity over southwest Asia using the Caspian Sea–Hindu Kush Index. Int. J. Climatol. http://dx.doi.org/10.1002/joc.5053.
Kaufman, Y.J., Tanré, D., Remer, L.A., Vermote, E.F., Chu, A., Holben, B.N., 1997. Operational remote sensing of tropospheric aerosol over land from EOS moderate resolution imaging spectroradiometer. J. Geophys. Res. 102, 17–51.
Knippertz, P., 2008. Dust emissions in the West African heat trough—the role of the diurnal cycle and of extratropical disturbances. Meteorol. Z 17 (5), 553–563.
Knippertz, P., Todd, M.C., 2010. The central west Saharan dust hot spot and its relation to African easterly waves and extratropical disturbances. J. Geophys. Res. 115, D12117. http://dx.doi.org/10.1029/2009JD012819.
Lavaysse, C., Flamant, C., Janicot, S., Parker, D.J., Lafore, J.-P., Sultan, B., Pelon, J., 2009. Seasonal evolution of the West African heat low: a climatological perspective. Clim. Dyn. 33, 313–330.

Lavaysse, C., Flamant, C., Janicot, S., 2010a. Regional-scale convection patterns during strong and weak phases of the Saharan heat low. Atmos. Sci. Lett. 11, 255–264. http://dx.doi.org/10.1002/asl.284.

Lavaysse, C., Flamant, C., Janicot, S., Knippertz, P., 2010b. Links between African easterly waves, mid-latitude circulation and the intra seasonal pulsations of the West African Heat Low. Quart. J. Roy. Meteor. Soc. 136, 141–158. http://dx.doi.org/10.1002/qj.555.

Lavaysse, C., Eymard, L., Flamant, C., Karbou, F., Mimouni, M., Saci, A., 2013. Monitoring the West African heat low at seasonal and intra-seasonal timescales using AMSU-A sounder. Atmos. Sci. Lett. 14, 263–271.

Marconi, M., Sferlazzo, D.M., Becagli, S., Bommarito, C., Calzolai, G., Chiari, M., di Sarra, A., Ghedini, C., Gómez-Amo, J.L., Lucarelli, F., Meloni, D., Monteleone, F., Nava, S., Pace, G., Piacentino, S., Rugi, F., Severi, M., Traversi, R., Udisti, R., 2014. Saharan dust aerosol over the central Mediterranean Sea: PM10 chemical composition and concentration versus optical columnar measurements. Atmos. Chem. Phys. 14, 2039–2054. http://dx.doi.org/10.5194/acp-14-2039-2014.

Marsham, J.H., Hobby, M., Allen, C.J.T., Banks, J.R., Bart, M., Brooks, B.J., Cavazos-Guerra, C., Engelstaedter, S., Gascoyne, M., Lima, A.R., Martins, J.V., McQuaid, J.B., O'Leary, A., Ouchene, B., Ouladichir, A., Parker, D.J., Saci, A., Salah-Ferroudj, M., Todd, M.C., Washington, R., 2013. Meteorology and dust in the central Sahara: observations from Fennec supersite-1 during the June 2011 intensive observation period. J. Geophys. Res. 118, 4069–4089. http://dx.doi.org/10.1002/jgrd.50211.

Marticorena, B., Chatenet, B., Rajot, J.L., Traoré, S., Coulibaly, M., Diallo, A., Koné, I., Maman, A., NDiaye, T., Zakou, A., 2010. Temporal variability of mineral dust concentrations over West Africa: analyses of a pluriannual monitoring from the AMMA Sahelian Dust Transect. Atmos. Chem. Phys. 10, 8899–8915. http://dx.doi.org/10.5194/acp-10-8899-2010.

Middleton, N.J., Goudie, A.S., 2001. Saharan dust: sources and trajectories. Trans. Inst. Br. Geogr. 26, 165–181. http://dx.doi.org/10.1111/1475-5661.00013.

Mona, L., Amodeo, A., Pandolfi, M., Pappalardo, G., 2006. Saharan dust intrusions in the Mediterranean area: three years of Raman lidar measurements. J. Geophys. Res. 111, D16203. http://dx.doi.org/10.1029/2005JD006569.

Morcrette, J.-J., Boucher, O., Jones, L., Salmond, D., Bechtold, P., Beljaars, A., Benedetti, A., Bonet, A., Kaiser, J.W., Razinger, M., Schulz, M., Serrar, S., Simmons, A.J., Sofiev, M., Suttie, M., Tompkins, A.M., Untch, A., 2009. Aerosol analysis and forecast in the ECMWF integrated forecast system. Part I: forward modelling. J. Geophys. Res. 114, D06206. http://dx.doi.org/10.1029/2008JD011235.

Morcrette, J.-J., Benedetti, A., Jones, L., Kaiser, J.W., Razinger, M., Suttie, M., 2011. Prognostic Aerosols in the ECMWF IFS: MACC vs. GEMS Aerosols, vol. 659. ECMWF Tech Memo available at: http://old.ecmwf.int/publications/library/ecpublications/_pdf/tm/601–700/tm659.pdf. (Accessed 4 November 2014).

Moulin, C., Lambert, C.E., Dayan, U., Masson, V., Ramonet, M., Bousquet, P., Legrand, M., Balkanski, Y.J., Guelle, W., Marticorena, B., Bergametti, G., Dulac, F., 1998. Satellite climatology of African dust transport in the Mediterranean atmosphere. J. Geophys. Res. 103, 13137–13144.

Nakamae, K., Shiotani, M., 2013. Interannual variability in Saharan dust over the North Atlantic Ocean and its relation to meteorological fields during Northern winter. Atmos. Res. 120, 336–346.

Pérez García-Pando, C., Stanton, M.C., Diggle, P.J., Trzaska, S., Miller, R.L., Perlwitz, J.P., Baldasano, J.M., Cuevas, E., Ceccato, P., Yaka, P., Thomson, M.C., 2014. Soil dust aerosols and wind as predictors of seasonal meningitis incidence in Niger. Environ. Health Perspect. 122, 679–686. http://dx.doi.org/10.1289/ehp.1306640.

Perry, K.D., Cahill, T.A., Eldred, R.A., Dutcher, D.D., Gill, T.E., 1997. Long-range transport of North African dust to the eastern United States. J. Geophys. Res. 102 (D10), 11225–11238. http://dx.doi.org/10.1029/97JD00260.

Prospero, J.M., Carlson, T.N., 1972. Vertical and areal distribution of Saharan dust over the western equatorial North Atlantic ocean. J. Geophys. Res. 77, 5255–5265.

Prospero, J.M., 1996. Saharan dust transport over the North Atlantic Ocean and mediterranean: an overview. In: Guerzoni, S., Chester, R. (Eds.), The Impact of Desert Dust across the Mediterranean, vol. 11. Kluwer Academic Publisher. http://dx.doi.org/10.1007/978-94-017-3354-0_13. Series Environmental Science and Technology Library, pp. 133–151, ISBN 978-94-017-3354-0,.

Prospero, J.M., 1999. Long-range transport of mineral dust in the global atmosphere: impact of African dust on the environment of the southeastern United States. PNAS 96 (7), 3396–3403. http://dx.doi.org/10.1073/pnas.96.7.3396.

Prospero, J.M., Ginoux, P., Torres, O., Nicholson, S., Gill, T., 2002. Environmental characterization of global sources of atmospheric soil dust identified with the NIMBUS7 Total Ozone Mapping Spectrometer (TOMS) absorbing aerosol product. Rev. Geophys. 40 (1), 1002. http://dx.doi.org/10.1029/2000RG000095.

Prospero, J.M., Lamb, P.J., 2003. African droughts and dust transport to the Caribbean: climate change implications. Science 302, 1024–1027. http://dx.doi.org/10.1126/science.1089915.

Prospero, J.M., Mayol-Bracero, O., 2003. Understanding the transport and impact of African dust on the Caribbean basin. Bull. Am. Meteorol. Soc. 94, 1329–1337. BAMS-D-12-00142.1, 2013.

Prospero, J.M., Collard, F.-X., Molinié, J., Jeannot, A., 2014. Characterizing the annual cycle of African dust transport to the Caribbean Basin and South America and its impact on the environment and air quality. Glob. Biogeochem. Cycles 29. http://dx.doi.org/10.1002/2013GB004802.

Ravelo-Pérez, L.M., Rodríguez, S., Galindo, L., García, M.I., Alastuey, A., López-Solano, J., 2016. Soluble iron dust export in the high altitude Saharan Air Layer. Atmos. Environ. 133, 49–59.

Roehrig, R., Chauvin, F., Lafore, J.-P., 2011. 10-25-Day intraseasonal variability of convection over the Sahel: a role of the Saharan heat low and midlatitudes. J. Clim. 24 (22), 5863–5878. http://dx.doi.org/10.1175/2011JCLI3960.1.

Rodríguez, S., Querol, X., Alastuey, A., Kallos, G., Kakaliagou, O., 2001. Saharan dust contributions to PM10 and TSP levels in Southern and Eastern Spain. Atmos. Environ. 35, 2433–2447.

Rodríguez, S., Alastuey, A., Alonso-Pérez, S., Querol, X., Cuevas, E., Abreu-Afonso, J., Viana, M., Pérez, N., Pandolfi, M., de la Rosa, J., 2011. Transport of desert dust mixed with North African industrial pollutants in the subtropical Saharan Air Layer. Atmos. Chem. Phys. 11, 6663–6685. http://dx.doi.org/10.5194/acp-11-6663-2011.

Rodríguez, S., Cuevas, E., Prospero, J.M., Alastuey, A., Querol, X., López-Solano, J., García, M.I., Alonso-Pérez, S., 2015. Modulation of Saharan dust export by the North African dipole. Atmos. Chem. Phys. 15, 7471–7486. http://dx.doi.org/10.5194/acp-15-7471-2015.

Sayer, A.M., Hsu, N.C., Bettenhausen, C., Jeong, M.-J., 2013. Validation and uncertainty estimates for MODIS Collection 6 "Deep Blue" aerosol data. J. Geophys. Res. Atmos. 118, 7864–7872. http://dx.doi.org/10.1002/jgrd.50600.

Schepanski, K., Tegen, I., Laurent, B., Heinold, B., Macke, A., 2007. A new Saharan dust source activation frequency map derived from MSG-SEVIRI IR-channels. Geophys. Res. Lett. 34, L18803. http://dx.doi.org/10.1029/2007GL030168.

Stein, A.F., Draxler, R.R., Rolph, G.D., Stunder, B.J.B., Cohen, M.D., Ngan, F., 2015. NOAA's HYSPLIT atmospheric transport and dispersion modeling system. Bull. Amer. Meteor. Soc. 96, 2059–2077.

Sultan, B., Janicot, S., 2003. The West African monsoon dynamics. Part II: the "preonset" and "onset" of the summer monsoon. J. Clim. 16 (21), 3407–3427. http://dx.doi.org/10.1175/1520-0442(2003)016<3407:TWAMDP>2.0.CO;2.

Takemura, T., Okamoto, H., Maruyama, Y., Numaguti, A., Higurashi, A., Nakajima, T., 2000. Global three-dimensional simulation of aerosol optical thickness distribution of various origins. J. Geophys. Res. 105, 17853–17873. http://dx.doi.org/10.1029/2000JD900265.

Tanré, D., Kaufman, Y.J., Herman, M., Mattoo, S., 1997. Remote sensing of aerosol properties over oceans using the MODIS/EOS spectral radiances. J. Geophys. Res. 102, 16971–16988. http://dx.doi.org/10.1029/96JD03437.

Tegen, I., 2003. Modeling the mineral dust aerosol cycle in the climate system. Quat. Sci. Rev. 22, 1821–1834. http://dx.doi.org/10.1016/S0277-3791(03)00163-X.

Tegen, I., Fung, I., 1994. Modeling of mineral dust transport in the atmosphere: sources, transport, and optical thickness. J. Geophys. Res. 99, 22897–22914. http://dx.doi.org/10.1029/94JD01928.

Tegen, I., Torres, R., 2005. Global iron connections: desert dust, ocean biogeochemistry and climate. Science 308, 67–71.

Thomson, M.C., Molesworth, A.M., Djingarey, M.H., Yameogo, K.R., Belanger, F., Cuevas, L.E., 2006. Potential of environmental models to predict meningitis epidemics in Africa. Trop. Med. Int. Health 11, 781–788.

Todd, M., Cavazos-Guerra, C., 2016. Dust aerosol emission over the Sahara during summertime from cloud-aerosol lidar with orthogonal polarization (CALIOP) observations. Atmos. Environ. 128, 147–157.

Varga, G., Ùjvári, G., Kovács, J., 2014. Spatiotemporal patterns of Saharan dust outbreaks in the Mediterranean basin. Aeolian Res. 15, 151–160. http://dx.doi.org/10.1016/j.aeolia.2014.06.005.

Wang, W., Evan, A.T., Flamant, C., Lavaysse, C., 2015. On the decadal scale correlation between African dust and Sahel rainfall: the role of Saharan heat low–forced winds. Sci. Adv. 1 (9), e1500646. http://dx.doi.org/10.1126/sciadv.1500646.

Yu, H., Chin, M., Yuan, T., Bian, H., Remer, L.A., Prospero, J.M., Omar, A., Winker, D., Yang, Y., Zhang, Y., Zhang, Z., Zhao, C., 2015. The fertilizing role of African dust in the Amazon rainforest: A first multiyear assessment based on data from Cloud-Aerosol Lidar and Infrared Pathfinder Satellite Observations. Geophys. Res. Lett. 42, 1984–1991. http://dx.doi.org/10.1002/2015GL063040.